Influence of Microchannel Geometry on Device Performance and Electrophysiological Recording Fidelity During Long-Term Studies of Connected Neural Populations

Noah Goshi¹, Gregory Girardi¹, Felipe da Costa Souza², Alexander Gardner³, Pamela J. Lein², and Erkin Seker^{3,*}

Departments of ¹Biomedical Engineering, ²Molecular Biosciences, and ³Electrical and Computer Engineering, University of California, Davis, CA 95616

*Corresponding author: eseker@ucdavis.edu

Abstract

Compartmentalized microfluidic neural cell culture platforms, which physically separate axons from the neural soma using a series of microchannels, have been used for studying a wide range of pathological conditions and basic neuroscience questions. While each study has different experimental needs, the fundamental design of these devices has largely remained unchanged and a systematic study to establish long-term neural cultures in this format is lacking. Here, we investigate the influence of microchannel geometry and cell seeding density on device performance particularly in the context of long-term studies of synaptically-connected, yet fluidically-isolated neural populations of neurons and glia. Of the different experimental parameters, the microchannel height was the principal determinant of device performance, where the other parameters offer additional degrees of freedom in customizing such devices for specific applications. We condense the effects of these parameters into design rules and demonstrate their utility in engineering a microfluidic neural culture platform with integrated microelectrode arrays. The engineered device successfully recorded from primary rat cortical cells for 59 days *in vitro* with more than on order of magnitude enhancement in signal-to-noise ratio in the microchannels.

Introduction

The central nervous system (CNS) is extremely complex, with each neuron communicating with hundreds to thousands of other neurons via synaptic connections¹. In addition, glial cells are in constant contact with neurons, and any disruption or dysregulation within this highly interconnected system can lead to disease states. This high complexity and interconnectivity has led to disproportionally high failure rates of late phase clinical trials targeting neurological disorders². One common approach to overcome this challenge has been the development of organ-on-a-chip models with electrophysiological read-out capabilities,³ which can be used to gain a better understanding of specific cellular and molecular mechanisms behind many neurological and neurodegenerative diseases. These models aim to reduce the complexity of the system as compared to *in vivo* models, while still maintaining many of the critical characteristics of the *in vivo* microenvironment (e.g., presence of relevant glial cells, mature neuronal networks, and distinct neural populations), and thereby allow researchers to conduct highly directed cellular level experiments with increased physiological relevance.

One popular example of an organ-on-a-chip model to study the CNS was first described by Taylor *et al*,⁴ and involves the use of polydimethylsiloxane (PDMS) based microfluidic culture platforms to physically separate the cell bodies of neurons and their axons. These culture platforms consist of two large cell culture chambers (which house the cell somas) and are connected by an array of microchannels that, due to their

reduced height, only allow neurites to pass through. Additionally, fluidic isolation of one chamber (primary) can be achieved by increasing the volume of media in the opposing chamber (secondary), thereby driving a hydrostatic pressure driven flow through the microchannels counteracting any diffusion from the primary chamber to the secondary chamber. These devices were initially used to study isolated axons, along with their growth and regeneration following injury.⁵ Researchers have subsequently adapted the original design for use in myriads of other studies including the formation of directional neural networks,^{6–8} investigating the transport and propagation of neurodegenerative disease related proteins,^{9–14} studying the spread of glutamate-induced ecotoxicity,¹⁵ and the innervation of non-neuronal cell cultures.^{16,17} While many great insights have been gained from these studies, the fundamental design of the platform - in particular the geometry interconnecting microchannel array - has largely been unchanged and may not be suitable for every application, especially for chronic studies that are necessary for recapitulating mature neuronal networks.

We performed a meta-analysis of over 200 unique research articles using similar organ-on-a-chip devices and found that ~70% articles used devices with geometries identical to the original devices described by Taylor *et al*,^{4,5} irrespective of cell type (CNS vs PNS), presence of glial cells, and experimental objective (**Figure S1**). Additionally, for the studies that used microchannels with different dimensions, nearly all of them used devices with larger microchannels, and in general there was limited discussion regarding the change over the common microchannel dimension. In the original device, the microchannels were 3 μm x 8-10 μm (height x width), with lengths ranging from 150-900 μm.^{4,5} The small height of the microchannels was largely effective at preventing the soma of the neurons (with average diameter's ranging from 7-58 μm)¹⁸ from entering the microchannels, while allowing axons and dendrites (with diameters ranging 0.2-2.2 μm)^{18,19} to easily enter and traverse the channels. The range of lengths were used to differentiate axons from dendrites, as it was noted that dendrites were unable to fully pass through microchannels greater than 450 μm in length.⁵ Taken together, the meta-analysis suggests that the majority of researchers use the original device dimensions, and the reasons for using a specific channel dimensions are not often discussed, even though these dimensions likely play a significant role in the device function.

In this paper we investigate the influence of microchannel geometry on device performance particularly in the context of long-term studies (1+ month) of synaptically-connected yet fluidically-isolated neural populations. Compared to acute studies, maintaining fluidic isolation becomes much more challenging as the fluid flow through the microchannels that counteracts diffusion is no longer negligible and may significantly alter the concentration of effector molecules. Additionally, for long-term studies, the inclusion of glial cells in the neuronal culture has been shown to improve the overall health of the culture and neuron function.^{20,21} Of the different glial cells that are included in these mixed cultures, astrocytes, which contain fine processes with similar diameters to axons,²² are able to extend processes a significant distance into the microchannels, which may confound experimental results. Here, we cultured primary rat cortical neurons and astrocytes in microfluidic culture platforms with varying microchannel dimensions to systematically compare the influence of microchannel dimensions and initial seeding densities, on the fluidic properties of the platform and the ability for neurons, astrocytes, and nuclei to enter and cross through the microchannels. In addition, we study the influence of microchannel geometry on the electrophysiological recording fidelity. We demonstrate that

microchannel height has an outstanding impact on the fluidic properties of the platform, while the seeding density can be used to adjust the number of astrocyte processes entering the microchannels. Using this information, we designed platforms that enable chronic studies, and demonstrate that neural activity can be recorded from these platforms (from electrodes placed under the cell culture chambers and microchannels) for at least 59 days *in vitro* (DIV) with more than an order of magnitude enhancement in signal-to-noise ratio in microchannels and significantly higher number of active electrodes. This study demonstrates the importance that small changes in microchannel dimensions can have on the overall performance of commonly-used microfluidic neural cell culture platforms and concludes with considerations for designing similar organ-on-a-chip devices for long-term neural culture and electrophysiology.

Experimental

Microfluidic platform design and fabrication

Multiple microchannel platforms were designed in order to assess the influence of microchannel geometry on different properties of the device (**Figure 1A**). "Array" style devices were designed to investigate the cellular response to different microchannel geometries. Each array device contained 4, 25 microchannel arrays with widths of 2, 5, 10, and 15 μ m. Additionally, these devices were designed with microchannel lengths of 500, 1000, and 1500 μ m and heights of 1.5, 3, and 6 μ m. "Full" style devices were used to determine the influence of microchannel geometries (of a single channel width per device) on the fluidic properties of the devices. These devices each had 101 microchannels with dimensions of 10 μ m x 1000 μ m x 1.5 or 6 μ m (width x length x height). Finally, "MEA" style devices contained an array of 25 microchannels with dimensions of 5 or 10 μ m x 1000 μ m x 1.5 μ m (width x length x height), which were bonded over custom microelectrode arrays (MEAs) designed for integration into the microchannel devices.

The fabrication of the microfluidic platforms followed standard soft lithography techniques. Briefly, master molds containing the different platform geometries were fabricated by patterning two layers of SU-8 (Kayaku Advanced Materials) on a silicon wafer using standard photolithography techniques. The first layer defined the interconnecting microchannels and was fabricated using SU-8 6005 deposited with different spin rates to achieve a final thickness of 1.5, 3, or 6 µm. The second layer defined the cell culture chambers and was fabricated using SU-8 2050 with a final thickness of 75 µm. Following the patterning of the cell culture chamber layer, the master molds were hard-baked for 1 h at 250 °C. All dimensions of the microfluidic platform master molds were confirmed using a Bruker Dektak XT profilometer following the hard-bake.

The master molds were placed in a 100 mm-diameter (Ø) petri dish and premixed (1:10 w/w curing agent to base) polydimethylsiloxane (PDMS; Slygard 184, Dow Corning) was poured over the mold and placed in a vacuum chamber to remove any bubbles. The PDMS was then placed on a 90 °C hotplate for 2.5 h to cure. The PDMS platforms were removed from the master mold and fluidic ports to access the cell culture chambers were opened using a 3 mm Ø biopsy punch. For the "array" and "full" style devices, the PDMS platforms were reversibly bonded to poly-L-lysine (PLL) coated glass coverslips. PLL coating was done by incubating the 0.5 mg/mL PLL (Sigma) in B-buffer (3.1 mg/mL boric acid and 4.75 mg/mL borax, Sigma) for 4 h at 37 °C and 5% CO₂. The coverslips were then washed with sterile deionized (DI) water and air dried. To

produce reversibly bonded devices, the PDMS platforms were sterilized with 70% EtOH followed by treatment in an air plasma cleaner at 10 W for 2 min. The PDMS platforms were then sealed over the PLL coated glass coverslips and glass cloning cylinders (8 mm x 6 mm inner Ø, Sigma) were fixed over each of the fluidic ports using sterile vacuum grease (Dow Corning) to form the final device (**Figure 1B**).

Custom MEAs were designed and fabricated to be integrated into "MEA" style devices (Figure 1C). Each MEA contained an array of 8 microelectrodes in each cell culture chamber, and an array of 16 microelectrodes placed under the microchannels, with microelectrodes having a surface area of 400 µm². The electrodes and traces (250 nm-thick Au over a 160 nm-thick Cr adhesion layer) were sputter-deposited on borosilicate glass wafers (500 µm thick, University Wafers) and patterned using standard lift-off techniques. A 250 nm layer of SiO₂ was deposited via PECVD to serve as the insulation layer. Finally, the electrode sites were lithographically patterned and opened via a brief immersion in buffered oxide etch. To form the final integrated microfluidic device, the MEAs were treated with air plasma to be permanently bonded to the corresponding "MEA" style microfluidic platform. Both the MEA and PDMS platforms were sterilized with 70% EtOH and the surfaces were activated with air plasma at 10 W for 2 min. The MEA was then covered with 70% EtOH and the PDMS platform was placed over the MEA and aligned under a microscope. The aligned device was placed in a vacuum chamber for 1 h to remove the EtOH solution and permanently bond the MEA and PDMS platform. The bonded devices were then treated with air plasma at 30 W for 10 min to make the surfaces hydrophilic and glass cloning cylinders were fixed over the fluidic ports. Finally, PLL solution was added to the device and incubated for 4 h and washed with sterile DI water to coat the interior surfaces of the device.

Analytical and Computational Modelling of Fluid Flow

Analytical modeling of the fluidic properties of the devices was done using previously described electrical circuit analogies, treating the interconnecting microchannels as resistors and the open wells containing media as capacitors²³. The dimensions of the model were the same as the "full" device with 101 microchannels with widths of 10 µm and lengths of 1000 µm. An initial volume differential of 150 µL per cell chamber (75 µL per well) was used to drive the hydrostatic pressure-induced flow, which amounted to a height differential of ~2.65 mm using the 6 mm inner Ø of the cloning cylinders. Computational modeling was done using COMSOL Multiphysics 5.5 solving for the Navier-Stokes equations to model the pressure-driven flow through the microchannels in a 3D model of the "full" device. The volumetric flow rate through the microchannels was determined at steady state with an initial pressure differential corresponding to a volume differential of 150 µL across the chambers. Detailed descriptions of the analytical and computational models can be found in the Supplemental Information.

Primary cortical culture

All procedures involving animals were conducted in accordance with the National Institutes of Health Guide for the Care and Use of Laboratory Animals following protocols approved by the University of California, Davis Institutional Animal Care and Use Committee. Timed-pregnant Sprague-Dawley rats were purchased from Charles River Laboratory (Hollister, CA). All animals were housed in clear plastic shoebox cages containing corn cob bedding under constant temperature (22 ± 2 °C) and 12 h light-dark cycle. Food and water

were provided ad libitum. Primary cortical cultures were prepared from postnatal day 0 rat pups as previously described.²⁴ Neocortices from all pups in the litter were pooled and dissociated.

Prior to seeding PLL coated devices were covered with plating medium (PM) consisting of Neurobasal A culture medium supplemented with 2% B27 supplement, 1X GlutaMAX, 10% heat-inactivated horse serum, and 20 mM HEPES at pH 7.5 (all from ThermoFisher). Primary cortical cells were seeded in PM at a density of $3 \times 10^6 - 20 \times 10^6$ cells/mL by adding 20 μ L of the cell suspension to the upper well of each chamber and incubated at 37 °C for 4 h to allow the cells to flow into the chamber and adhere. For experiments quantifying the cellular response to microchannel geometry, only one chamber was seeded with cells, and the other chamber was loaded with 20 μ L of PM. Following the incubation, the excess PM and unattached cells were removed, and each well was filled with 150 μ L of growth medium (GM) consisting of Neurobasal A culture medium supplemented with 2% B27, 1X GlutaMAX (all from ThermoFisher). Half media changes were performed twice a week throughout the length of the experiments.

Immunocytochemistry

At the conclusion of the experiment, cell cultures were washed 3 times with 37 °C DPBS with calcium and magnesium (DPBS+) and fixed using 4% w/v paraformaldehyde (PFA; Affymetrix) in PBS for 2.5 h. For reversibly bonded devices, the PDMS overlay was removed and the glass coverslip with the fixed cells was washed 3 times with DPBS+ to remove any residual PFA. For permanently bonded devices, following fixation, the PFA was removed, and the devices were washed 3 times with DPBS+.

For reversibly bonded devices, the fixed cells were washed twice with 0.05% v/v Tween20 (Sigma) solution in DPBS+, followed by a 3 min permeabilization with 0.1% v/v Triton X-100 (ThermoFisher) solution in DPBS+ and two additional washes with Tween20/ DPBS+ solution. Samples were blocked with a solution of 0.5% v/v heat-inactivated goat serum (ThermoFisher) and 0.3 M glycine (Sigma) in DPBS+ (blocking buffer) for 1 h. Following the blocking step, samples were incubated for 1 h in primary antibody solution containing anti-βIII tubulin (ThermoFisher) and rabbit anti-GFAP (ThermoFisher) in blocking buffer. Samples were then washed 3 times with Tween20 solution before a 1 h incubation with secondary antibody solution containing goat anti-mouse antibodies conjugated to AlexaFluor 647 (ThermoFisher) and goat anti-rabbit antibodies conjugated to AlexaFluor 488 (ThermoFisher). Following incubation with secondary antibody solution, the samples were washed 3 times with DPBS+. Lastly, samples were incubated for 5 min with a 4',6-diamidino-2-phenylindole (DAPI) solution (1:20000 dilution in DI H₂0, Sigma), followed by an additional Tween20 solution wash before mounting onto glass slides using ProLong Gold Antifade Mountant (ThermoFisher).

For the permanently bonded devices, a similar methodology was followed, with increased incubation durations to ensure permeation of the reagents into the microchannels: (i) the permeabilization step was done with Tween20 solution with a 4 h incubation, (ii) the blocking step increased to an overnight incubation (18 h) at 4 °C, and (iii) the primary and secondary antibody incubation steps each increased to 72 h at 4 °C.

Quantification of cell culture response to microchannel geometry

To quantify the cellular response, primary cortical cells were cultured for 14 days in one chamber of the "array" style device and fixed and immunostained as described above. All sample images were acquired with a Zeiss Observer D1 inverted fluorescence microscope at 100x magnification and analyzed with ImageJ. Four

different responses were quantified by manually determining: (i) the number of microchannels with at least 1 axon crossing the entire length of the channel, (ii) the number of nuclei that entered or crossed through the microchannels, (iii) the number of channels that had at least 1 astrocyte process entering the channel, (iv) the length that the astrocyte process extended into the microchannels (**Figure 2**).

Electrophysiology recording and analysis

For electrophysiology measurements, the devices were placed on a custom-built rig and maintained at 37 °C and 5% CO₂ during the recordings. Recordings were performed at a sampling frequency of 30 kHz using an RHD2132 Intan amplifier (Intan Technologies). Half-media changes were performed 24 h prior to each recording.

Feature extraction from the recordings was done using Offline Sorter and NeuroExplorer (Plexon). Spikes were detected following a filtering (300 Hz high pass) using a threshold of 8x standard deviation of the noise. Channels that showed less than 10 spikes per 10 min recording were discarded from the analysis. The number of active electrodes for each array (or electrode position – i.e., placed under a 5 µm wide channel, 10 µm wide channel, or within the culture chamber) was determined as the number of electrodes with at least 10 spikes detected during the 10 min recording. Overall synchrony of the active electrodes within each device was determined using the SPIKE-distance methodology²⁵ using the PySpike Python package.²⁶ The following features were determined on a per electrode basis, but statistical analysis was performed on a per device basis by taking the overall mean from the active electrodes. The signal-to-noise ratio (SNR) and root mean (RMS) noise from each active electrode were automatically determined by Offline Sorter. Bursts were classified using the *max interval* method in NeuroExplorer using previously defined parameters.^{21,27} Briefly these parameters were; (i) maximum initial inter-spike interval (ISI) of 0.1 s, (ii) maximum end ISI of 0.25 s, (iii) minimum inter-burst interval of 0.8 s, (iv) minimum burst duration of 0.05 s, and (v) minimum number of spikes in bursts of 6 spikes. The percentage of total spikes within bursts, the average burst duration, and average ISI within bursts were also calculated at a per electrode basis.

Statistical analysis

Hierarchical linear regression was used to determine the most impactful predictor variables (3 microchannel dimensions and seeding density) on each of the 4 cellular responses. As all the predictor variables and responses showed a non-gaussian distribution, each was normalized prior to employing a forward stepwise linear regression analysis. To compare change in the different spike features based on electrode position, each data set was fitted using a linear mixed effects model (treating the individual devices as a random effect) with a b-spline basis to account for the overall shape of the plots. We then compared the estimated marginal means from the fitted curves at 3 pre-determined timepoints (7, 21, and 56 DIV) representing the early, middle, and late stages of the cultures and adjusted for multiple comparisons using Tukey's method. In all cases a p-value < 0.05 was considered significant. All statistical analyses were performed in R.

Results and Discussion

Cell culture response to different microchannel dimensions

In order to improve the long-term performance of microfluidic cell culture platforms that were used to study synaptically connected neural populations, we compared the response of the primary cortical cells cultured in "array" style devices to a number of different variables including microchannel width, length, and height along with the initial seeding density. One chamber of the device was seeded with 20 µL of cortical cells at high (20 x 10⁶ cells/mL) and low (3 x 10⁶ cells/mL) concentrations. A seeding volume of 20 µL was chosen as preliminary studies indicated that higher seeding volumes lead to a more even distribution of cells within the chamber, without altering the plating density. Nevertheless, multiple designs of each "array" style device were fabricated, in which the order of arrays of microchannels were randomly placed along the device to account for any uneven distribution of seeding density. The cortical cells in these devices were maintained for 14 DIV, after which they were fixed, and the different culture responses were quantified.

Axon crossing microchannels

One critical parameter determining the functionality of these organ-on-a-chip devices is the ability for axons to cross through the microchannels and thereby synaptically connect the two neural populations. Our results indicate that for most microchannel geometries, by DIV 14 axons are able to consistently cross through all available microchannels, especially at higher seeding densities (**Figure 3a**). However, we observe a clear reduction in the number of microchannels with axon crossings at small channel widths (2 µm) and long channel lengths (1500 µm), which is exacerbated at low seeding densities. These observations were confirmed by hierarchical regression analysis (**Figure 4a**), which indicates that the most significant variables, in order of importance, were seeding density, microchannel width, and microchannel length. Interestingly, microchannel height, while still significantly improving the adjusted R² coefficient of the regression model, had the least impact on the ability for axons to cross through the microchannels (**Figure 3a & 4a**). It has been shown that axons from cortical neurons have heights of less than 1 µm when cultured on planar surfaces, ²⁸ and therefore axons were not physically excluded from the microchannels even at the lowest tested height. Additionally, while percentage of microchannels with at least one axon crossing did not substantially increase as microchannel widths increased above 5 µm, we did observe that microchannels with increased widths had a larger number of axons crossing through each individual microchannel.

Soma confinement in chambers

The ability to effectively confine the somas from each cell population to their respective chamber is another critical aspect to the effectiveness of these devices. Although the height of the most reported microchannel geometries are smaller than the size of neurons and glial cells (**Figure S1**), there are a number of reports of showing significant populations of neurons or glial cells that pass through similarly designed microchannels.^{29–32} We found that microchannel height had a significant impact on the soma confinement capabilities of the device (**Figure 3b**) and was the most significant factor in explaining the observed variance (**Figure 4b**). Additionally, increasing the seeding density ubiquitously increased the number of non-confined cells across all conditions, and was the second most important factor identified by hierarchical regression analysis (**Figure 3b & 4b**). For devices seeded at 20 x 10⁶ cells/mL the average number of non-confined cells

averaged across all microchannel widths and lengths, were 0.25 ± 0.65 , 31.78 ± 30.28 , and 145.36 ± 161.93 for devices with microchannel heights of 1.5, 3, and 6 µm respectively. These values dropped to 0.21 ± 0.44 , 4.28 ± 7.29 , and 19.29 ± 24.20 when the initial seeding density was reduced to 3×10^6 cells/mL. Microchannel width and length also played a significant role in determining the effectiveness of the cellular confinement of the devices, but their effect was only observed at larger channel heights and higher seeding densities (**Figure 3b & 4b**).

Interestingly, while we initially expected to see similar numbers of cells entering or crossing through the microchannels with similar cross-sectional areas (i.e., 5 µm wide x 6 µm tall vs 10 µm wide x 3 µm tall), we observed that microchannel height plays a substantially greater role in determining if cell nuclei can enter the microchannels. Microchannels with heights of 1.5 µm showed a near complete confinement of nuclei within the seeded cell culture chamber, regardless of seeding density or other microchannel dimensions. It has been shown that nuclei in cultured cells can undergo large deformations in width and length to pass through confined microchannels but show a lesser ability to adjust nuclei height.³³ It has also been shown that compressing the nuclei of HeLa cells below 3.5 µm leads to nuclear lamina rupture, nuclear blebbing, and alterations in gene expression.³⁴ This suggests that for these devices, reducing microchannel heights below 3 um may be an effective way to ensure near total confinement of cells within their seeded chambers. Additionally, we observed that the loss of somal confinement occurred rapidly following cell seeding, most likely due to cells flowing into the channels during the initial seeding. This observation is supported by comparing the overall ratio of neurons to astrocytes that were not confined to the seeded cell chamber. Averaged across all conditions, the ratio of neurons to total cells was 0.92 ± 0.08. While it has been shown that small populations of cultured neurons can migrate in response to specific stimuli, the large majority of cultured neurons are considered non-motile. 35,36 Conversely, astrocytes have been shown to migrate readily even in the absence of stimulation,³⁷ and therefore we would expect a higher ratio of non-confined astrocytes to neurons if post-seeding migration was dominant. This suggests that cell confinement may not be a critical factor if each chamber is seeded with cells from the same initial population, however in instances where two distinct cell populations are seeded in opposing chambers, reducing microchannel height to prevent cellular crosscontamination is critical.

Astrocytes permeating microchannels

Many studies have demonstrated that culturing neurons with other glial cells can improve the overall health of the neuronal cultures especially at later timepoints (> 28 DIV). 20,21,38 Previous studies along with our own preliminary experiments indicated that microglia, mature oligodendrocytes (OLs), and oligodendrocyte precursor cells (OPCs) do not interact significantly with the microchannels, 39-41 however astrocytes are able to extend processes significant distances into the microchannels. Therefore, we wanted to quantify the astrocyte response to different microchannel geometries. We observed that seeding density was the primary factor in determining the percentage of microchannels containing at least one astrocyte process (**Figure 3c & 4c**), accounting for nearly 50% of the variance. As astrocytes account for only ~20% of the cells seeded, it is unsurprising that increasing the number of astrocytes close to the microchannels has the largest effect. The addition of microchannel width, length, and height to the regression model each improves the adjusted R²

value of the model by a statistically significant amount (**Figure 4c**), where microchannel height had the least impact on the ability for astrocyte processes to enter the channel. Similar to axons, this is most likely due to the fact that cultured astrocytes have an average height of less than 1 μ m,²² and therefore would largely be unaffected by the reduction in channel height. All four parameters significantly influenced the length that astrocyte processes extended into the microchannel, but compared to the other culture responses, the proportion of the variance explained by these four parameters was substantially less (adj R² for the full model = 0.11) (**Figure 4d**). However, we observed that astrocytes were able to extend processes up to ~450 μ m into the microchannels with the largest cross-sectional areas (6 μ m x 15 μ m). This suggests that when co-culturing neurons and astrocytes together in these devices, microchannel lengths should be a minimum of 1000 μ m to prevent the formation of astrocyte-astrocyte gap junctions, which may confound experimental results that assume only synaptic connectivity between the chambers.

Influence of microchannel height on the stability of soluble factor concentrations in the chambers

In addition to the cellular response, the fluidic properties of these microfluidic neural culture platforms can be significantly altered by small changes in microchannel geometry. While many papers using these devices highlight and employ the fluidic isolation capabilities of these devices, the volume of fluid flow between the cell culture chambers required to counteract diffusion and maintain fluidic isolation is less studied. While at short time scales (minutes to hours), effects of this fluid flow are negligible, at longer timescales (days to weeks) this fluid flow may significantly alter the concentration of soluble factors (e.g., pharmaceuticals) added to the fluidically isolated chamber. In order to study this, we estimated the fluid flow through the microchannels using an electric circuit analog. We determined that of the three microchannel dimensions, microchannel height had the largest influence on the estimated fluid flow. This is largely due to the cubic relationship between the height of a rectangular microchannel and its hydraulic resistance. Table 1 shows the estimated volumetric flow rate through "full" style devices (10 µm width x 1000 µm length, with 101 microchannels) with varying heights and an initial volume differential of 75 µL per well or ~2.65 mm difference in height. When the microchannel height was increased to 5 µm, ~18 µL flowed between the chambers within only 24 h. While this volume appears negligible, the volume of each cell culture chamber of the full device is ~2.45 µL, resulting in the entire volume of the cell culture chamber being overturned every ~3.25 hours. We also estimated the volumetric flow rate through the microchannels using a 3D computational model of the "full" style device using COMSOL Multiphysics 5.5 (Table 1). The COMSOL simulation showed a good agreement with the electrical circuit analogy. The higher values estimated by the COMSOL model can be attributed to the fact that the COMSOL model was solved for steady-state, and thus the pressure between the chambers did not decrease with the change in volume differential.

In order to experimentally confirm the results from the electric circuit analog and computational model, that is, whether dilution of the treatment chamber soluble factors is significant due to the media flow, we seeded primary cortical cells at a density of 3 x 10^6 cells/mL in both cell culture chamber of "full" style devices with microchannel heights of 1.5 μ m and 6 μ m. After allowing the cells to adhere, 150 μ L of GM was added to each well connected to the "secondary" chamber, while 75 μ L GM with 50 μ M cytosine arabinoside (AraC) was added to each well connected to the "treatment" chamber. The devices were maintained for 48 h with no media

changes, after which they were fixed and immunostained. At this concentration AraC acts as a neurotoxic factor,⁴² and thus we would expect to see significant neuron death in the treatment chambers. As expected, we observed significant neural death in the treatment chamber of microfluidic platforms with microchannel heights of 1.5 µm, however we did not see any neural death in the treatment chambers of the devices with microchannel heights of 6 µm (Figure 5a). In order to quantify neuronal cell viability, we compared the percent area of each field-of-view stained for β-III tubulin with a circularity less than 0.2 using ImageJ (**Figure 5b**). The circularity cutoff was used to eliminate the contribution of cell debris from apoptotic/necrotic neurons, which still stained for β-III tubulin, but lacked long cellular processes, and therefore had high circularity values. A two-way ANOVA indicated a significant interaction between chamber (treatment vs secondary) and microchannel height on the percent area covered by neurons (p = 0.0095). Analysis of the simple main effects (using Tukey's method to account for multiple comparisons) revealed a significantly reduced percent area coverage of neurons in the treatment chamber as compared to the secondary chamber in the devices with a 1.5 µm microchannel height (p = 0.0057). However, in the devices with 6 µm tall microchannels, we observed no significant difference (p = 0.99) in the neuron percent area coverage, indicating that the flow between the chambers was enough to "wash-out" the AraC from the treatment chamber preventing the neurotoxic effect. Additionally, we did not see a significant difference in the neuron coverage between the control chambers of the different devices (p = 0.85) indicating that reducing microchannel height does not negatively influence the fluidic isolation of the treatment chamber. We have observed similar results from established (DIV 14) cultures in devices with 1.5 µm tall channels, with severe neuronal death isolated to the treatment chamber following a 4 day excitotoxic challenge, whereas cultures in devices with 6 µm tall channels show no cell death in either chamber (Figure S2). These results indicate that reducing the height of the microchannels can significantly improve the fluidic properties of these devices, especially during extended treatment times. Furthermore, as half-media changes are required every 3-4 days to maintain the cultures, it is expected that the robust fluidic isolation observed in the 1.5 µm microchannel height devices can be maintained indefinitely, as the volume differential between the chambers can naturally be "reset" every 3-4 days. Finally, axonal growth into the channels likely further improves the fluidic isolation between the chambers by reducing the effective channel cross-section available for fluid flow, that is, increasing the hydraulic resistance.

An alternative method to reduce the flow between the chambers during fluidic isolation that has been used by some researchers is decreasing the volume difference between the control and treatment chambers. While this method is effective in reducing the fluid flow by reducing the pressure differential, we found that this comes at the expense of fluidic isolation (**Figure S3**). We observed a similar reduction in fluid flow between the chambers by reducing the hydrostatic pressure differential in devices with 6 μ m tall microchannels to ~0.71 mm as compared to devices with 1.5 μ m tall microchannels with a more standard hydrostatic pressure differential (~2.83 mm). However, we also observed diffusion of dye molecules from the treatment chambers within the microchannels of the reduced-volume differential devices. This was not observed in devices with 1.5 μ m or 6 μ m tall microchannels that maintained the more standard hydrostatic pressure differential. This suggests that reducing microchannel height as opposed to reducing the hydrostatic

pressure differential is the better solution to reduce the fluid flow through the microchannels when absolute fluidic isolation of the treatment chamber is critically important.

Influence of microchannel geometry of electrophysiological recording fidelity

Extracellular recording from neural cultures seeded onto MEAs in a well format have been widely used to study the development of neural circuit activity and responses to various pharmaceutical and pathological stimuli.43 Similarly, MEAs can be integrated into microfluidic neural culture devices to record neural activity from synaptically-connected neural populations along with the interconnecting axons. While most research in this area has primarily been to demonstrate the ability to record large single unit recordings from axons within microchannel^{44–46} or study the rate of action potential (AP) propagation along axons, ^{47,48} some researchers have begun to study the electrophysiological response of neurons cultured in these chambers to compartmentalized treatments^{49,50} or develop directional neural networks.^{51,52} For studying connected neural populations for longer durations (1+ month), it is necessary to determine the impact on microchannel geometry on electrophysiological recording fidelity. We seeded primary cortical cells at a concentration of 3 x 10⁶ cells/mL and cultured them in "MEA" style devices integrated with a 32 channel MEA (16 electrodes were placed under the microchannels, and 8 were placed in each chamber) (Figure 1c). Based on our previous results, we narrowed down the fabricated devices to two microchannel geometries. All microchannels had lengths of 1000 µm to prevent astrocyte gap junction formation between the chambers and heights of 1.5 µm to minimize cell nuclei entering the chambers and improve fluidic isolation, informed by the studies above. The devices contained microchannels with either 5 µm or 10 µm channel widths, and the dimensions of the corresponding electrodes were adjusted to ensure a 400 µm² exposed electrode area. Additionally, the number of microchannels in the device was reduced from 101 to 25 and the surface area of each cell culture chamber was reduced to increase the likelihood of neurons attaching close to the chamber electrodes.

At DIV 59 the cultures maintained within the devices appeared healthy with robust neural processes and non-activated astrocyte morphologies²⁰ (Figure 6a) and showed robust neural activity recorded from electrodes in both the chamber (Figure 6b) and under the microchannels (Figure 6c). Initially, the percentage of active electrodes (electrodes recording at least 10 spikes during the 10 min recording) increased for all electrode types (electrodes placed under 10 µm-wide microchannels, 5 µm-wide microchannels, and within cell culture chambers), with almost 100% active channels by DIV 17 for the microchannel electrodes (Figure 6d). This increased percentage of active electrodes in the microchannels is likely due to the microchannels guiding the axons directly over the electrode sites, eliminating the stochastic effect of neuron-electrode proximity required for electrodes in the chambers. At early (DIV 7) and middle (DIV 21) timepoints when the cultures are maturing and reaching maturity respectively, there is no difference between the percentage of active channels in 10 µm and 5 µm wide microchannels (p = 0.48 at DIV 7 & p = 0.59 at DIV 21). However, the percentage of active electrodes begin to decline at a much more rapid rate for 5 µm-wide microchannel electrodes as compared to electrodes under the 10 µm-wide channels, and by DIV 56 we observe a significant difference in the percent active electrodes (p < 0.0001). The decline in the number of active channels over time is not unexpected as it has been shown that the overall health of primary cortical cultures begins to decline around 28-35 DIV.^{21,53} We expect that over time the axons in the microchannel may begin to deteriorate as the overall

health of the neuron declines, and as the 10 μ m-wide microchannels contain more axons, this decrease is less pronounced as recording neural activity from only a single healthy axon is required to classify an electrode as active.

We see a similar relationship between electrode types when comparing changes in spike frequency (**Figure 6e**). Once again, for microchannels, there is an initial increase in firing rate as the culture matures followed by a decrease as the culture ages. The significant differences in estimated marginal means at DIV 21 between the microchannel and chamber electrodes (p < 0.0001 for both 5 µm and 10 µm microchannels) can be attributed to recording from multiple axons within the microchannels. This also supports previous studies that show the AP from one axon within a microchannel does not depolarize other axons within the microchannel. Unlike the number of active channels, there was no difference in firing rate between the 5 µm and 10 µm-wide microchannels at DIV 56 (p = 0.32). This difference can partially be attributed to the fact that non-active channels were excluded from the spike frequency analysis, and therefore contributions from rapidly degrading axons were not included in the analysis. Unlike the recordings from the microchannels, the firing rate of neurons in the chamber was relatively stable following the initial rise as the culture matured. This indicates that the neurons in the culture chambers may remain relatively healthy, but over time a portion of the axons within the microchannels begin the degrade.

We report significant increases in SNR (**Figure 6f**) and noise (**Figure 6g**) from electrodes within the microchannels as compared to those in the cell culture chambers. This is in line with previous reports showing increased SNR and noise floors from electrodes placed within microchannels. ^{45–47} The increase in noise can largely be attributed to the increase in electrode impedance due to the added electrical resistance along the length of the microchannel. ⁴⁵ Similarly the increased resistance in the microchannel due to the spatial confinement leads to an increase in the spike amplitude. ⁴⁶ Additionally, large numbers of neurites and astrocytes can block both sides of the microchannels essentially creating a high-resistance seal, which can dramatically increase the spike amplitude and lead to the much larger SNR seen in the microchannels (with a roughly order of magnitude difference at DIV 21). ⁴⁶ Interestingly, we saw a decrease in SNR over time in the 5 µm microchannels that was not observed in the 10 µm microchannels. As the microchannel geometries do not change over the course of the experiment, this may be attributed to a loss of the high-resistance seal in the 5 µm microchannels.

We also compared a number of different electrophysiological features (percentage of spikes in bursts, within burst ISI, and burst duration) to assess culture maturation and stability over time (**Figure 7a-c**). As expected, we see an increase in the percentage of spikes in bursts across all electrode types as the cultures mature. Additionally, over time we see a similar change in the percent of spikes in bursts as with the firing rate. Within microchannels, the percentage of spikes in bursts begins to decrease, presumably as some axons within the microchannels begin to degrade. In contrast, within the chamber, the values remain relatively constants, again suggesting that the neurons in the culture chambers remain healthy over the extended culture times. We also observe minimal changes over time for the within-burst ISI and burst duration, which also suggests that the cultures are healthy over the 59 DIV.

Finally, we compared the overall synchrony in devices with 5 μ m and 10 μ m-wide channels to assess the network development and stability over time (**Figure 7d**). We calculated the overall synchrony by comparing the dissimilarity of the spike trains of active channels using the SPIKE-distance method^{25,26} (with values closer to 1 indicating higher levels of synchronization between the spike trains of active channels). While we observed an increase in synchrony for both devices as the cultures matured, the devices with 10 μ m-wide channels reached a higher degree of synchronization (p = 0.035 at DIV 56). This is presumably due to the increased number of axons crossing through the wider microchannels and form a more robust network between the two separated chambers. We also observed that for both devices the synchrony plateaued following the initial rise, suggesting that the network is stable over the extended culture times. Overall, these results suggest that increasing microchannel width may improve network formation between the microchannels and improve electrophysiological recording fidelity within the microchannels.

Conclusions

In this study, we have demonstrated the significant impact of small changes in microchannel geometry can have on the overall device functionality of commonly used microfluidic neural culture platforms. In particular, we studied how microchannel geometry influenced the cellular confinement, axon crossings, fluidic properties, and electrophysiological recording fidelity when using these devices. It is important to note that all experiments in this study were performed using cortical cells from neonatal rats. While the size distribution of neurons and astrocytes in mice and rats are similar, the axon diameter and overall astrocyte size of human cells tends to skew slightly larger. 19,54–56 As the size difference between neuronal cells from rodents and humans are relatively minimal (for example over 95% axons from rat, 19 mouse, 54 and human 66 cortical neurons are less than 1.5 µm) we do not expect the cell source to significantly impact the results from this study. Additionally, as both human neurons and astrocytes are larger than their rodent counterparts, the overall conclusions drawn from this study should remain applicable across species. Below, we describe how each design factor can influence device functionality and summarize general design rules for different experimental objectives (**Figure 8**).

i) **Microchannel Height:** It is best to keep microchannel height as small as possible, ideally around 1.5 μm. Reducing microchannel heights to this value significantly reduces the number of cell bodies that can enter the microchannels (improving cellular confinement) while minimally impacting the ability for axons to enter the channels. Additionally, there is a significant reduction in the volumetric flow rate through the microchannels when a hydrostatic pressure differential is maintained. This is especially critical for long-term studies, where fluid flow between the chambers can significantly alter the concentration of soluble factors added to the fluidically isolated chamber. In general, we do not recommend increasing microchannel height above 1.5 μm, with the exception that if peripheral neurons are being cultured taller microchannels may be required to accommodate the larger axon diameters.⁵⁷ In this case the initial seeding density should be reduced to minimize the number of cells

that enter the microchannels, and treatment times should be kept to a minimum to minimize changes in the effector molecule concentration.

- ii) **Microchannel Length:** For long-term experiments studying connected neural populations, in which both neurons and astrocytes will be added to both sides of the microchannels, it is important that the microchannels are at least 1000 μm in length to prevent the formation of astrocyte-astrocyte gap junctions within the microchannels. For experiments in which cells are cultured on only one side of the microchannels or when only neurons are being cultured, the previous recommended length of 450-500 μm should be used to prevent dendrites from crossing through the channels.⁴
- iii) **Microchannel Width:** For extended studies of connected neural populations, we suggest a microchannel width of at least 5 μm to ensure robust connectivity between the chambers. Increasing microchannel width beyond 5 μm can improve the long-term electrophysiological recording fidelity, at the cost of increasing the number of axons in each microchannel. If robust synaptic connectivity between the chambers is desired, increasing the number of axons in each microchannel is beneficial and there is little to no drawback from increasing microchannel width. If the experiment requires a single axon to be present in each microchannel (i.e., single axon imaging or electrophysiological recording studies) reducing the microchannel width down to 2 μm may be worthwhile. If this is the case, increasing the initial seeding density can be used to counteract the reduced axon crossings and improve the overall connectivity between the chambers.
- iv) Initial Seeding Density: The initial seeding density can largely be used as a tool or countermeasure to reduce some of the negative side effects of altering microchannel geometries. Increasing seeding density can be used to increase the number of axons crossing the microchannels when using devices with small microchannel widths or very long microchannel lengths. Alternatively, reducing the seeding density can improve the cellular confinement of devices with large microchannel heights. Additionally, reducing initial seeding density can substantially reduce the number of astrocyte processes within the microchannels.

Author Contributions

NG and ES designed the experiments. NG performed device fabrication, cell culture, electrophysiological recordings, imaging, and data analysis and wrote the main manuscript text. GG contributed to the development and fabrication of microfluidic devices and microelectrode arrays, and data analysis. FDCS contributed to the development of the cell culture. AG contributed to electrophysiological data analysis. ES and PJL contributed to the interpretation of experimental results and edited the manuscript. All authors read and approved the final manuscript.

Conflicts of Interest

The authors declare no conflicts of interest.

Acknowledgements

We gratefully acknowledge the support from the National Institutes of Health via NINDS/NIA R03-NS118156, NIBIB R21-EB024635, and NCCIH R21-AT010933, and from the National Science Foundation via CBET-1454426 and DMR-2003849. NG was partially supported by the UC Davis Biotechnology Training Program award. This project benefited from the resources of the MIND Institute IDDRC Core services (NICHD P50-HD103526) and University of California, Davis - Center for Nano/Micro-Manufacturing facility.

References

- 1 R. Yuste, *Nat. Rev. Neurosci.*, 2015, **16**, 487–497.
- D. E. Pankevich, B. M. Altevogt, J. Dunlop, F. H. Gage and S. E. Hyman, *Neuron*, 2014, **84**, 546–553.
- 3 Y. Berdichevsky, J. Staley and M. L. Yarmush, 2010, 999–1004.
- 4 A. M. Taylor, S. W. Rhee, C. H. Tu, D. H. Cribbs, C. W. Cotman and N. L. Jeon, *Langmuir*, 2003, **19**, 1551–1556.
- 5 A. M. Taylor, M. Blurton-Jones, S. W. Rhee, D. H. Cribbs, C. W. Cotman and N. L. Jeon, *Nat. Methods*, 2005, **2**, 599–605.
- A. Virlogeux, E. Moutaux, W. Christaller, A. Genoux, J. Bruyère, E. Fino, B. Charlot, M. Cazorla and F. Saudou, *Cell Rep.*, 2018, **22**, 110–122.
- J. M. Peyrin, B. Deleglise, L. Saias, M. Vignes, P. Gougis, S. Magnifico, S. Betuing, M. Pietri, J. Caboche, P. Vanhoutte, J. L. Viovy and B. Brugg, *Lab Chip*, 2011, **11**, 3663–3673.
- A. Iannielli, G. S. Ugolini, C. Cordiglieri, T. Cabassi, M. Rasponi, V. Broccoli, A. Iannielli, G. S. Ugolini, C. Cordiglieri, S. Bido, A. Rubio, G. Colasante, M. Valtorta, T. Cabassi, M. Rasponi and V. Broccoli, *CellReports*, 2019, **29**, 4646–4656.
- J. C. Polanco, C. Li, N. Durisic, R. Sullivan and J. Götz, *Acta Neuropathol. Commun.*, 2018, **6**, 10.
- L. Urrea, M. Segura-Feliu, M. Masuda-Suzukake, A. Hervera, L. Pedraz, J. M. García Aznar, M. Vila, J. Samitier, E. Torrents, I. Ferrer, R. Gavín, M. Hagesawa and J. A. del Río, *Mol. Neurobiol.*, 2018, **55**, 1847–1860.
- 11 M. Brahic, L. Bousset, G. Bieri, R. Melki and A. D. Gitler, *Acta Neuropathol.*, 2016, **131**, 539–548.
- 12 S. Akira and K. Takeda, *Nat. Rev. Immunol.*, 2004, **4**, 499–511.
- S. Takeda, S. Wegmann, H. Cho, S. L. Devos, C. Commins, A. D. Roe, S. B. Nicholls, G. A. Carlson, R. Pitstick, C. K. Nobuhara, I. Costantino, M. P. Frosch, D. J. Muller, D. Irimia and B. T. Hyman, *Nat. Commun.*, DOI:10.1038/ncomms9490.
- 14 H. L. Song, S. Shim, D. H. Kim, S. H. Won, S. Joo, S. Kim, N. L. Jeon and S. Y. Yoon, *Ann. Neurol.*, 2014, **75**, 88–97.
- 15 A. J. Samson, G. Robertson, M. Zagnoni and C. N. Connolly, Sci. Rep., 2016, 6, 1–11.
- 16 K. A. Southam, A. E. King, C. A. Blizzard, G. H. McCormack and T. C. Dickson, *J. Neurosci. Methods*, 2013, **218**, 164–169.
- J. Bellmann, R. Y. Goswami, S. Girardo, N. Rein, Z. Hosseinzadeh, M. R. Hicks, V. Busskamp, A. D. Pyle, C. Werner and J. Sterneckert, *Biomaterials*, 2019, **225**, 119537.

- 18 J. C. Fiala and K. M. Harris, in *Dendrites* 2, 1999, pp. 1–11.
- 19 G. Partadiredja, R. Miller and D. E. Oorschot, *J. Neurocytol.*, 2003, **32**, 1165–1179.
- N. Goshi, R. K. Morgan, P. J. Lein and E. Seker, J. Neuroinflammation, 2020, 17, 1–16.
- H. A. Enright, D. Lam, A. Sebastian, A. P. Sales, J. Cadena, N. R. Hum, J. J. Osburn, S. K. G. Peters, B. Petkus, D. A. Soscia, K. S. Kulp, G. G. Loots, E. K. Wheeler and N. O. Fischer, *Sci. Rep.*, 2020, **10**, 1–14.
- V. M. Tiryaki, V. M. Ayres, I. Ahmed and D. I. Shreiber, *Nanomedicine*, 2015, **10**, 529–545.
- 23 G. Robertson, T. J. Bushell and M. Zagnoni, *Integr. Biol.*, 2014, **6**, 636–644.
- G. A. Wayman, D. D. Bose, D. Yang, A. Lesiak, D. Bruun, S. Impey, V. Ledoux, I. N. Pessah and P. J. Lein, *Environ. Health Perspect.*, 2012, **120**, 1003–1009.
- T. Kreuz, D. Chicharro, C. Houghton, R. G. Andrzejak and F. Mormann, *J. Neurophysiol.*, 2013, **109**, 1457–1472.
- 26 M. Mulansky and T. Kreuz, *SoftwareX*, 2016, **5**, 183–189.
- P. Charlesworth, E. Cotterill, A. Morton, S. G. N. Grant and S. J. Eglen, *Neural Dev.*, 2015, **10**, 1–10.
- P. Froeter, Y. Huang, O. V. Cangellaris, W. Huang, E. W. Dent, M. U. Gillette, J. C. Williams and X. Li, *ACS Nano*, 2014, **8**, 11108–11117.
- L. Vitzthum, X. Chen, D. B. Kintner, Y. Huang, S. Y. Chiu, J. Williams and D. Sun, *Integr. Biol.*, 2010, **2**, 58–64.
- 30 R. K. Pirlo, A. J. Sweeney, B. R. Ringeisen, M. Kindy and B. Z. Gao, *Biomicrofluidics*, , DOI:10.1063/1.3552998.
- 31 L. Li, L. Ren, W. Liu, J. C. Wang, Y. Wang, Q. Tu, J. Xu, R. Liu, Y. Zhang, M. Sen Yuan, T. Li and J. Wang, *Anal. Chem.*, 2012, **84**, 6444–6453.
- 32 A. Bastiaens, R. Sabahi-Kaviani and R. Luttge, *Front. Neurosci.*, 2020, **14**, 1–11.
- 33 M. T. Doolin, T. S. Ornstein and K. M. Stroka, *Cells*, 2019, **8**, 1–17.
- 34 M. Le Berre, J. Aubertin and M. Piel, *Integr. Biol. (United Kingdom)*, 2012, **4**, 1406–1414.
- T. N. Behar, S. V. Smith, R. T. Kennedy, J. M. Mckenzi, I. Maric and J. L. Barker, *Cereb. Cortex*, 2001,
 11, 744–753.
- 36 M. A. Haas, J. A. Chuckowree, R. S. Chung, J. C. Vickers and T. C. Dickson, *Cell Motil. Cytoskeleton*, 2007, **64**, 274–287.
- 37 E. A. Lepekhin, C. Eliasson, C. H. Berthold, V. Berezin, E. Bock and M. Pekny, *J. Neurochem.*, 2001,

- **79**, 617–625.
- 38 D. Majumdar, Y. Gao, D. Li and D. J. Webb, *J. Neurosci. Methods*, 2011, **196**, 38–44.
- 39 J. Park, H. Koito, J. Li and A. Han, *Lab Chip*, 2012, **12**, 3296–3304.
- 40 S. Hosmane, I. H. Yang, A. Ruffin, N. Thakor and A. Venkatesan, *Lab Chip*, 2010, **10**, 741–747.
- 41 H. U. Lee, S. Nag, A. Blasiak, Y. Jin, N. Thakor and I. H. Yang, *ACS Chem. Neurosci.*, 2016, **7**, 1317–1324.
- 42 D. P. Martin, T. L. Wallace and E. M. Johnson, *J. Neurosci.*, 1990, **10**, 184–193.
- 43 M. V. Accardi, M. K. Pugsley, R. Forster, E. Troncy, H. Huang and S. Authier, *J. Pharmacol. Toxicol. Methods*, 2016, **81**, 47–59.
- 44 N. Hong, S. Joo and Y. Nam, *IEEE Trans. Biomed. Eng.*, 2017, **64**, 492–498.
- L. Pan, S. Alagapan, E. Franca, T. Demarse, G. J. Brewer and B. C. Wheeler, *IEEE Trans. Neural Syst. Rehabil. Eng.*, 2014, **22**, 453–459.
- 46 L. Wang, M. Riss, J. O. Buitrago and E. Claverol-tintur, , DOI:10.1088/1741-2560/9/2/026010.
- 47 M. K. Lewandowska, D. J. Bakkum, S. B. Rompani and A. Hierlemann, *PLoS One*, 2015, **10**, 1–24.
- 48 K. Shimba, K. Sakai, K. Arimatsu, K. Kotani and Y. Jimbo, *Int. IEEE/EMBS Conf. Neural Eng. NER*, 2013, 945–948.
- 49 R. Habibey, A. Golabchi, S. Latifi, F. Difato and A. Blau, *Lab Chip*, 2015, **15**, 4578–4590.
- 50 M. K. Lewandowska, M. Radivojević, D. Jäckel, J. Müller and A. R. Hierlemann, *Front. Neurosci.*, , DOI:10.3389/fnins.2016.00083.
- G. J. Brewer, M. D. Boehler, S. Leondopulos, L. Pan, S. Alagapan, T. B. DeMarse and B. C. Wheeler, Front. Neural Circuits, 2013, **7**, 1–8.
- 52 T. Honegger, M. A. Scott, M. F. Yanik and J. Voldman, *Lab Chip*, 2013, **13**, 589–598.
- C. A. R. Chapman, L. Wang, H. Chen, J. Garrison, P. J. Lein and E. Seker, *Adv. Funct. Mater.*, 2016, 1604631, 1604631.
- 54 C. L. Call and D. E. Bergles, *Nat. Commun.*, DOI:10.1038/s41467-021-25035-2.
- 55 B. Zhou, Y. X. Zuo and R. T. Jiang, *CNS Neurosci. Ther.*, 2019, **25**, 665–673.
- D. Liewald, R. Miller, N. Logothetis, H. J. Wagner and A. Schüz, *Biol. Cybern.*, 2014, **108**, 541–557.
- 57 M. Ristola, L. Sukki and M. M. Azevedo, *J. Micromechanics Microengineering*.

Figures and Captions

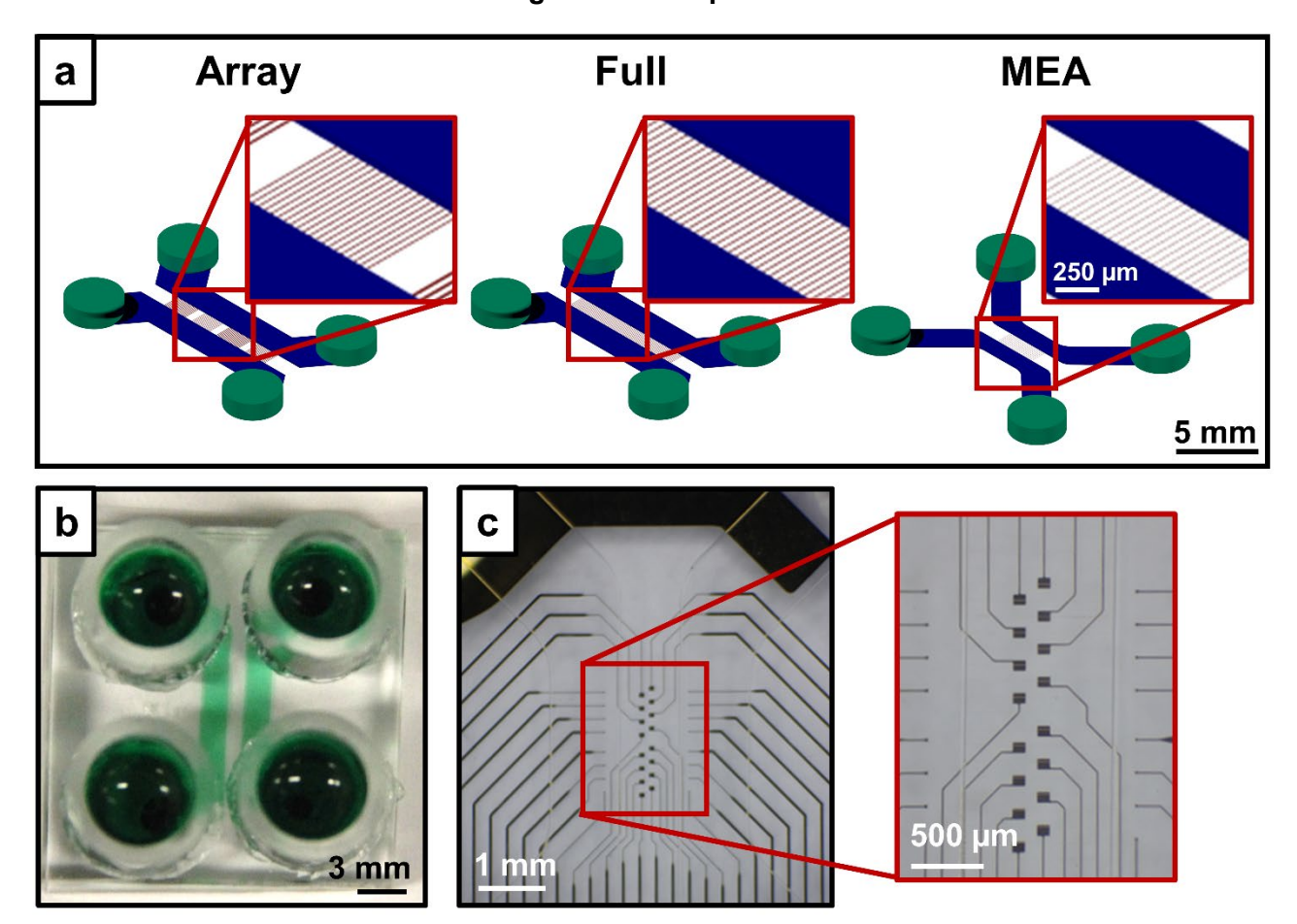


Figure 1: Examples of different microfluidic platforms used in this study. (a) 3D renderings of the three styles of microfluidic platforms. The microchannels are shown in red with dimensions of 1.5-6 μm x 2-15 μm x 500-1500 μm (height x width x length) depending on the design. The cell culture chambers are shown in blue with a height of 75 μm. The fluidic access ports are shown in green and created via biopsy punch (3 mm \emptyset) over which glass cloning cylinders (6 mm \emptyset , 8 mm height) were affixed to increase the overall media volume capacity. (b) An example of a fully assembled device with affixed cloning cylinders. (c) An example of an "MEA" style device with the integrated MEA.

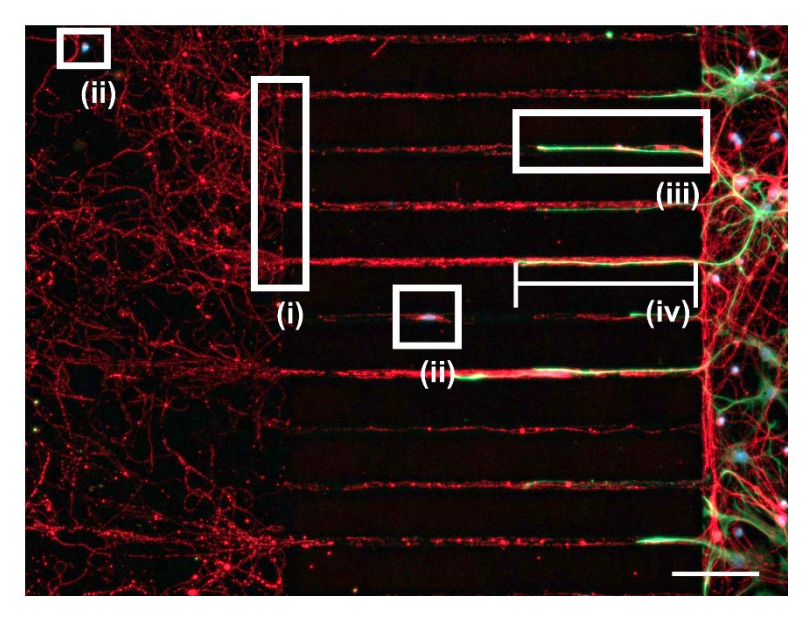


Figure 2: Representative fluorescence image illustrating the different cellular responses to varying device parameters. The cultures were immunostained for neurons – anti- β III-tubulin (red) and astrocytes – anti-GFAP (green) and the general nuclear stain DAPI (blue). The responses quantified are as follows: (i) the number of microchannels with at least 1 axon crossing the entire length of the channel, (ii) the number of nuclei that entered or crossed through the microchannels, (iii) the number of channels that had at least 1 astrocyte process entering the channel, (iv) the length that the astrocyte process extended into the microchannels. Scale bar = 100 μ m.

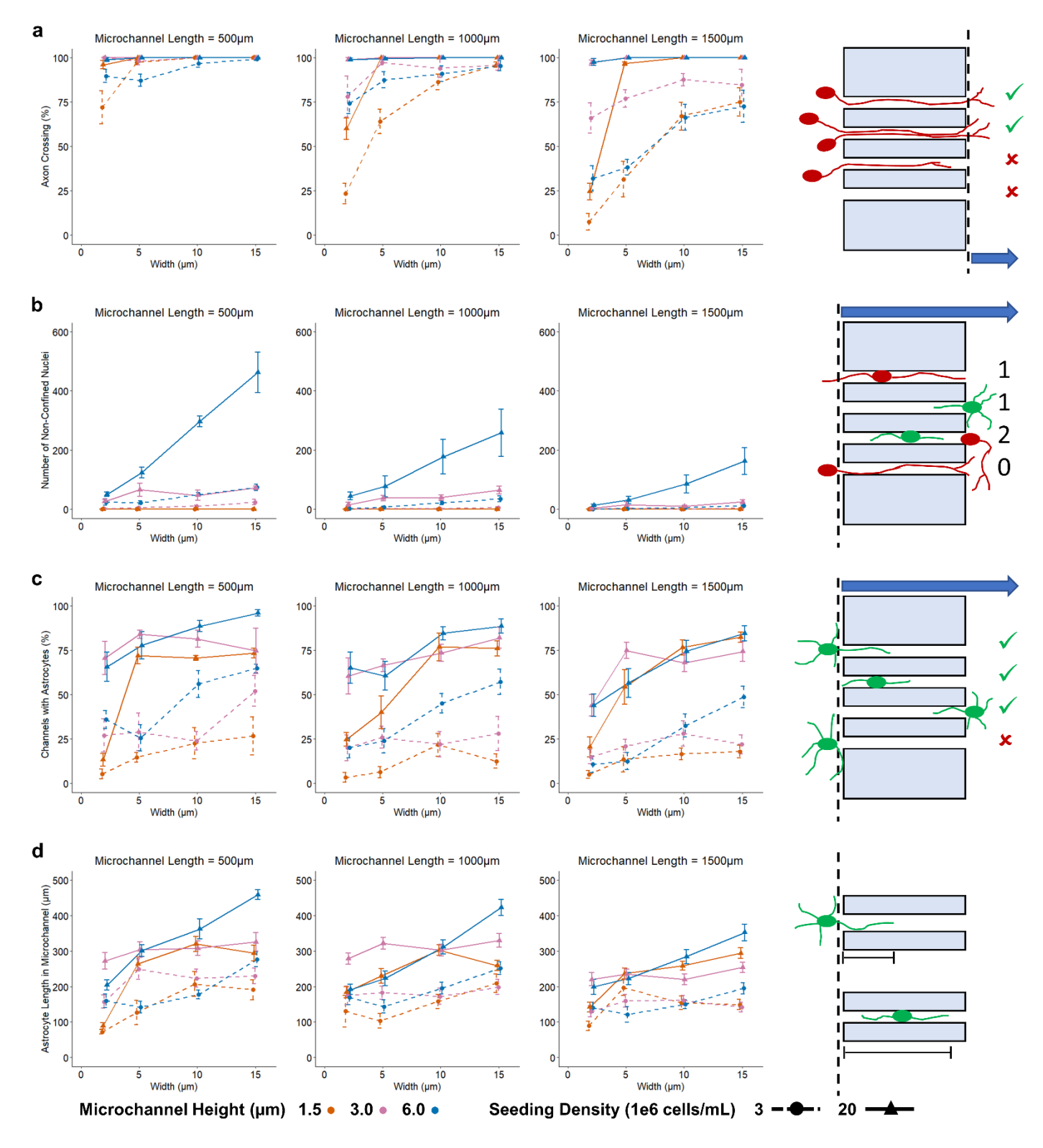


Figure 3: Quantification of (a) the percentage of microchannels with at least one axon crossing the entirety of the channel, (b) The number of non-confined cell bodies (nuclei), (c) the percentage of microchannels that contained at least one astrocyte process, and (d) the length that the astrocyte process extended into the microchannels to varying device parameters (mean \pm SEM, n = 4-8 from two independent dissections). For the quantification of astrocyte length, only channels that contained at least one astrocyte process were analyzed. A schematic representation of how each response was quantified is shown in the right-most column.

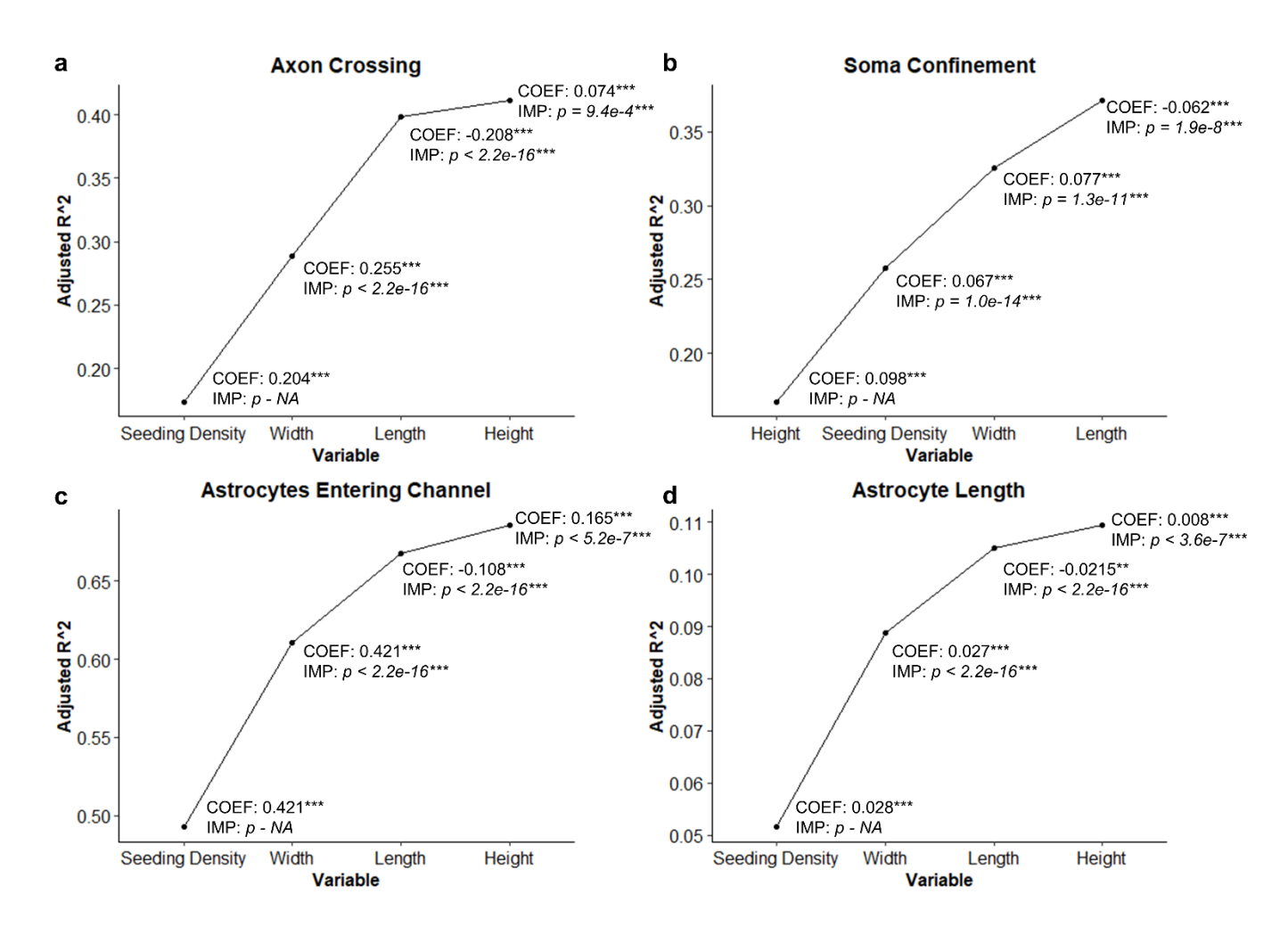


Figure 4: Plots showing the change in the adjusted R^2 following the addition of each variable in the stepwise linear regression model for (a) the percentage of microchannels with at least one axon crossing fully through the microchannel, (b) the number of nuclei not confined to the initial seeding chamber, (c) the number of microchannels with at least one astrocyte process in them, and (d) the length that the astrocyte process extended into a microchannel. IMP indicates the *p-value* for the improvement in adjusted R^2 due to the addition of the respective variable. COEF indicates the coefficient of that variable in the full model with all four variables included. *p < 0.05, **p < 0.01, ****p < 0.001

Channel Height (µm)	Q (μL/day) Circuit Analogy	Q (μL/day) COMSOL
1	0.20	0.20
2	1.48	1.57
5	18.19	22.58

Table 1: Estimated volumetric flow rate for the first 24 h given by electrical circuit analogy or 3D computational model (COMSOL).

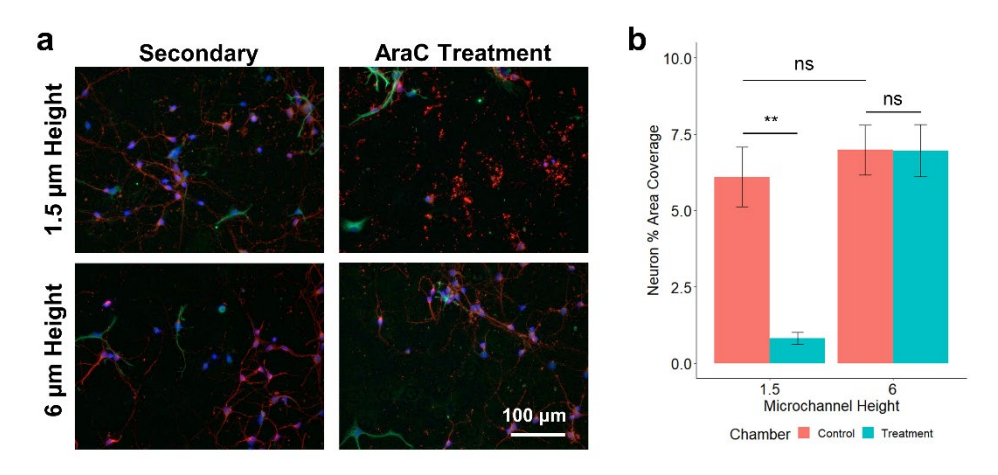


Figure 5: (a) Representative fluorescence images from the different cell culture chambers following 48 h exposure to 50 μM AraC in the treatment chamber. The cultures were immunostained for neurons – anti-βIII-tubulin (red) and astrocytes – anti-GFAP (green) and the general nuclear stain DAPI (blue). (b) Quantification of the percent area coverage of neurons with a circularity cutoff of 0.2 to eliminate cellular debris (mean \pm SEM, n = 3 from two independent dissections). **p < 0.01.

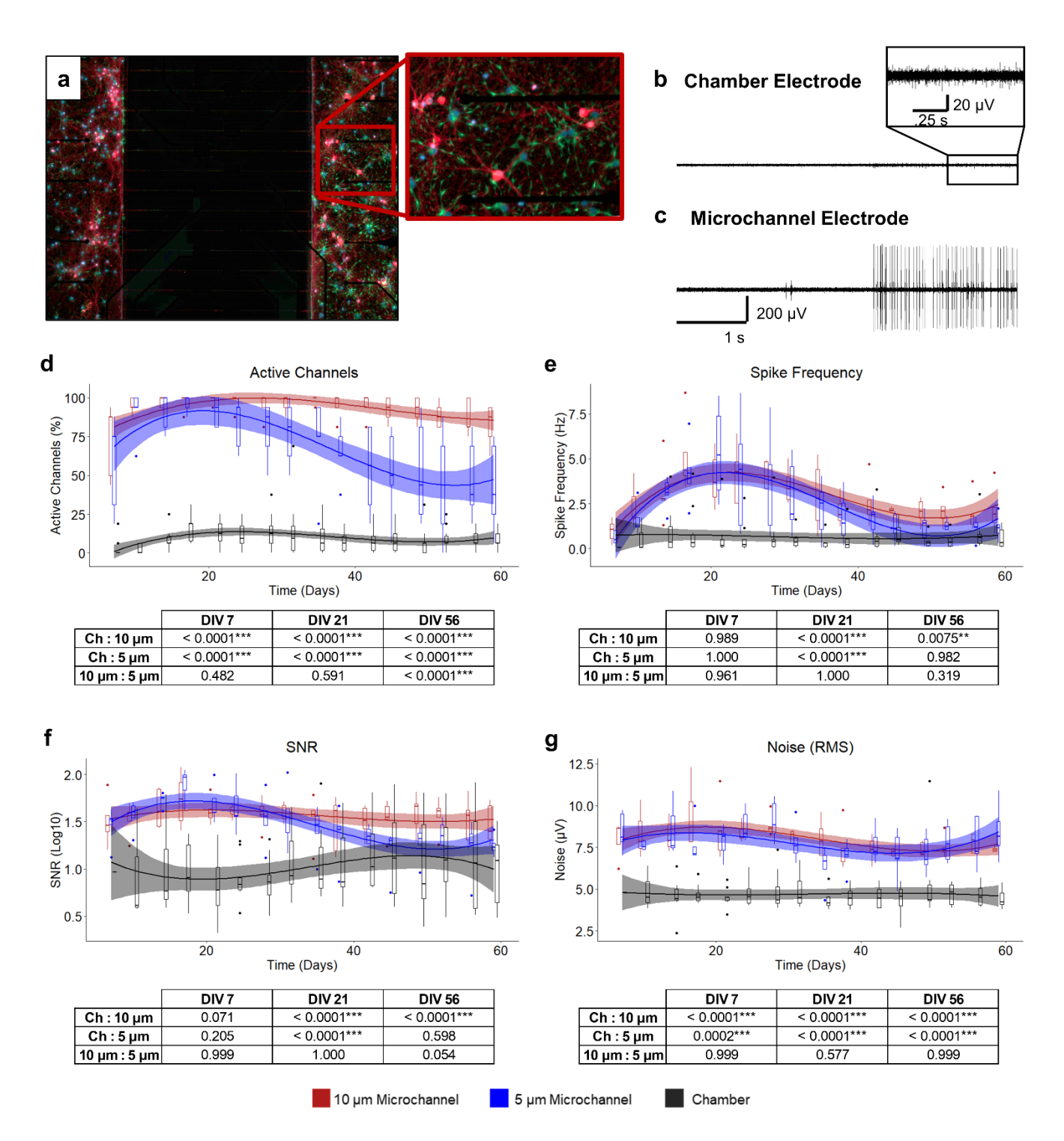


Figure 6: (a) Representative fluorescence image of cortical cells cultured in the "MEA" style device for 59 DIV. The cultures were immunostained for neurons – anti-βIII-tubulin (red) and astrocytes – anti-GFAP (green) and the general nuclear stain DAPI (blue). Representative recordings taken at DIV 59 from an electrode placed (b) within the cell culture chamber and (c) under a microchannel. Comparisons of the (d) percent active channels, (e) spike frequency, (f) SNR, and (g) RMS noise from electrodes placed under 10 μm wide microchannels (red), 5 μm wide microchannels (blue), and within the cell culture chambers (black). The solid lines show the fitted linear mixed effects model (treating the individual devices as a random effect) with a b-spline basis. The shaded regions are the 95% confidence interval. The tables show the p-values comparing the estimated marginal means of the fitted curves at pre-determined timepoints. (n = 5, from two independent dissections). ***p < 0.01, ***p < 0.001

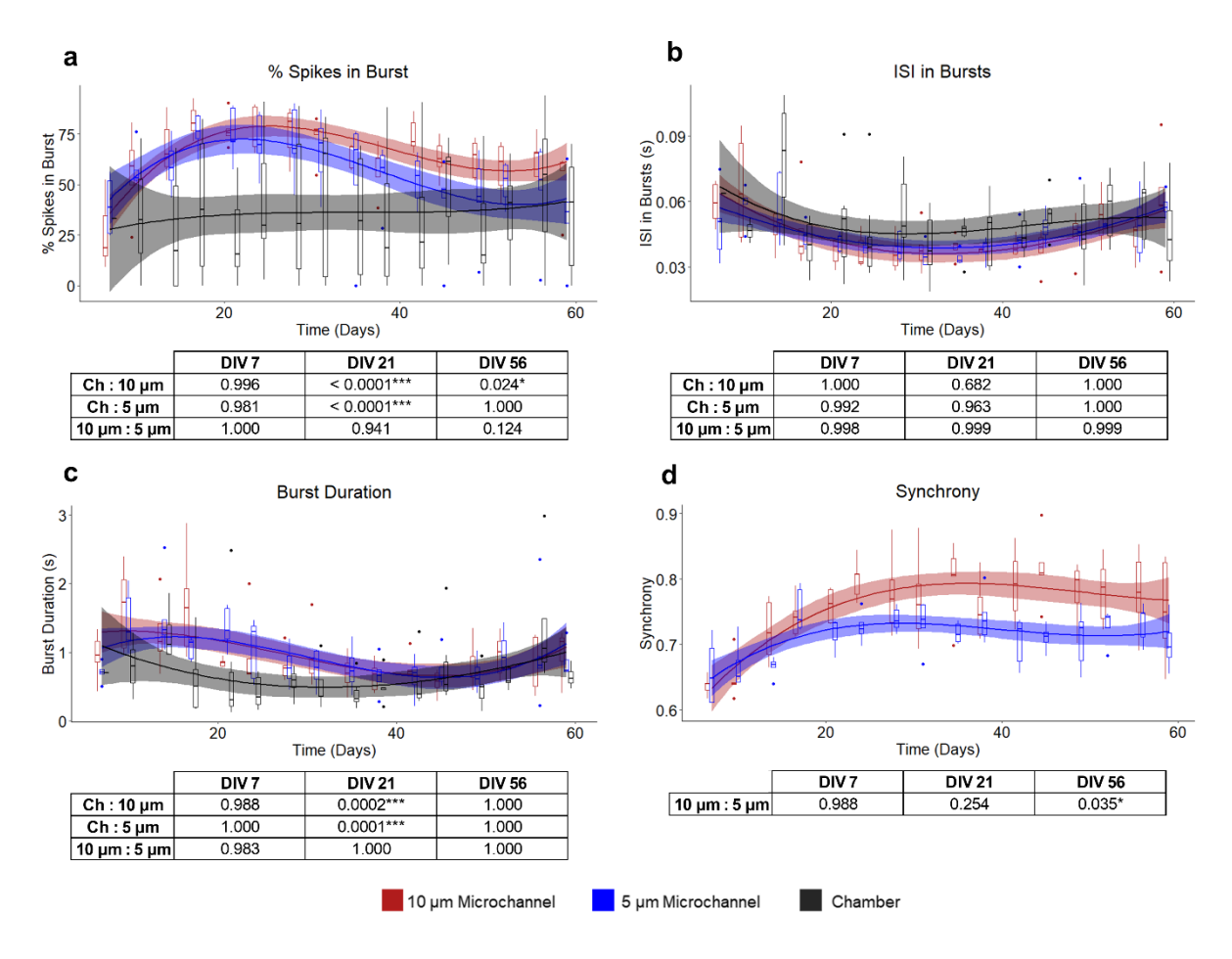


Figure 7: Comparisons of the (a) percentage of total spikes in bursts, (b) within-burst ISI, and (c) burst duration from electrodes placed under 10 μm wide microchannels (red), 5 μm wide microchannels (blue), and within the cell culture chambers (black). (d) Comparing the overall synchrony in devices with 10 μm-wide microchannels (red) and 5 μm-wide microchannels (blue). The solid lines show the fitted linear mixed effects model (treating the individual devices as a random effect) with a b-spline basis. The shaded regions are the 95% confidence interval. The tables show the p-values comparing the estimated marginal means of the fitted curves at pre-determined timepoints. (n = 5, from two independent dissections). *p < 0.05, **p < 0.01, ***p < 0.001.

Microchannel Height

- Should be minimized to improve the fluidic properties of the device and limit the number of cell bodies that can enter the microchannels.
- A microchannel height of 1.5 µm is ideal for CNS cultures.
- For PNS cultures taller channels may be required to allow for the larger axon diameters of PNS neurons.



Microchannel Width

- Should be adjusted depending on the experimental objective.
- Small microchannel widths reduce the connectivity between chambers but, increase the probability of axonal connectivity.
- Larger microchannel widths increase axonal connectivity between the chambers and improve long term electrophysiological recording fidelity, but most microchannels will contain more than one axon.



Microchannel Length

- Should be adjusted depending on the experimental objective.
- Microchannel length should be at least 1000 µm to prevent astrocyteastrocyte gap junctions from forming when studying connected mixed neuron-glia cultures.
- Microchannel length should be at least 450 µm to prevent dendrites from crossing between chambers.



Seeding Density

- Should be adjusted to compensate for previous design choices.
- Increasing seeding density will increase the number of in each microchannel and increase axonal connectivity between chambers.
- Decreasing seeding density will reduce the number of cell bodies and astrocyte processes entering the microchannels.

Figure 8: A summary of general step-wise design rules for different experimental objectives.

Supporting Information

Influence of Microchannel Geometry on Device Performance and Electrophysiological Recording Fidelity During Long-Term Studies of Connected Neural Populations

Noah Goshi¹, Gregory Girardi¹, Felipe da Costa Souza², Alexander Gardner³, Pamela J. Lein², and Erkin Seker^{3,*}

Departments of ¹Biomedical Engineering, ²Molecular Biosciences, and ³Electrical and Computer Engineering, University of California, Davis, CA 95616

*Corresponding author: eseker@ucdavis.edu

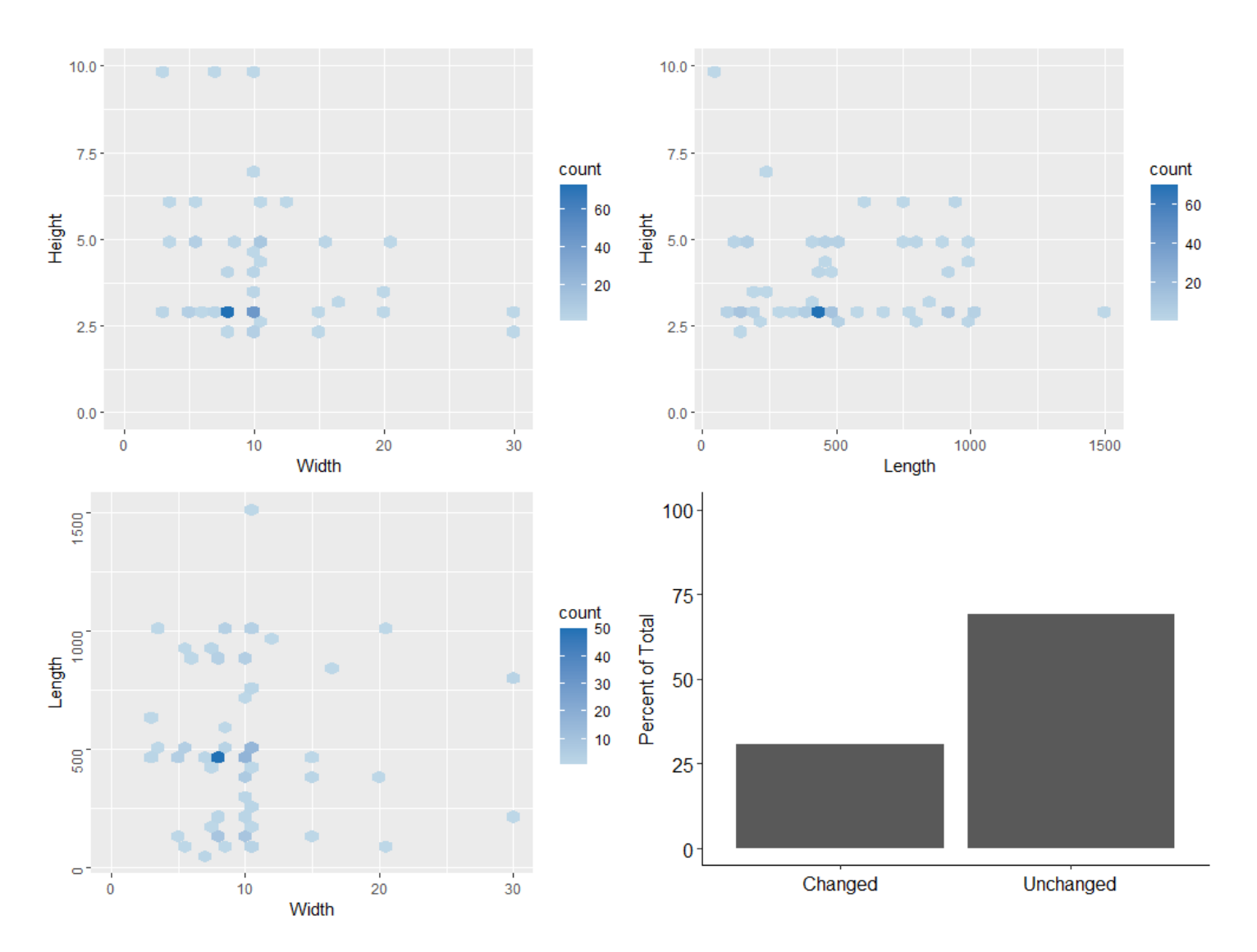


Figure S1: Analysis of different microchannel dimensions reported in publications using "axon compartmentalization" style microfluidic devices. Most common microchannel dimensions were 3 μ m x 8 μ m x 450 μ m (H x W x L), which are the original dimensions reported by Taylor *et al* and are the dimensions of commercially available devices (Xona Microfluidics), with ~70% of all studies use microchannel dimensions of 3 μ m x 8 μ m x 450-1000 μ m. The bottom-right plot illustrates the percentage of the cited papers that use the same original dimensions or different dimensions than the original. (A full list of references used to generate this data is listed at the end of the Supporting Information).

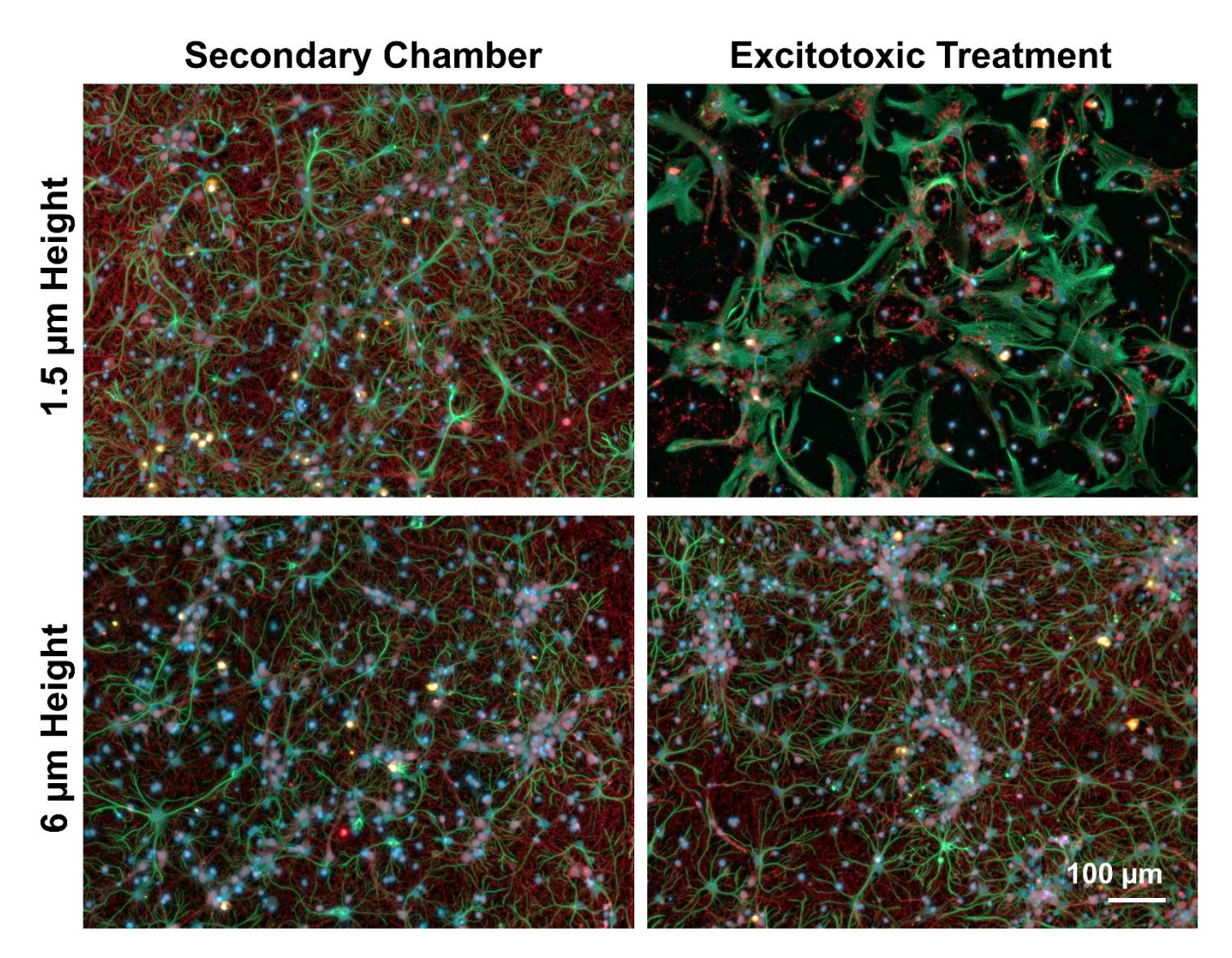


Figure S2: Representative fluorescence images from the different cell culture chambers following a 4-day excitotoxic treatment (100 μM glutamate). These cultures were maintained using a previously described triculture medium, ¹ which maintains a small number of microglia in addition to neurons and astrocytes within the culture. For the device with 1.5 μm-high channels, the flow from the secondary chamber to the treatment chamber did not dilute the added glutamate in the treatment chamber; hence, excitotoxic injury was observed (e.g., severe neural death and astrocyte hypertrophy). However, for the device with the 6 μm-high channels, the excessive flow from the secondary chamber to the treatment chamber diluted the glutamate to the extent that no excitotoxic effect was observed in the treatment culture. The cultures were immunostained for neurons – anti-βIII-tubulin (red), astrocytes – anti-GFAP (green), microglia – anti-Iba1 (orange), and the general nuclear stain DAPI (blue).

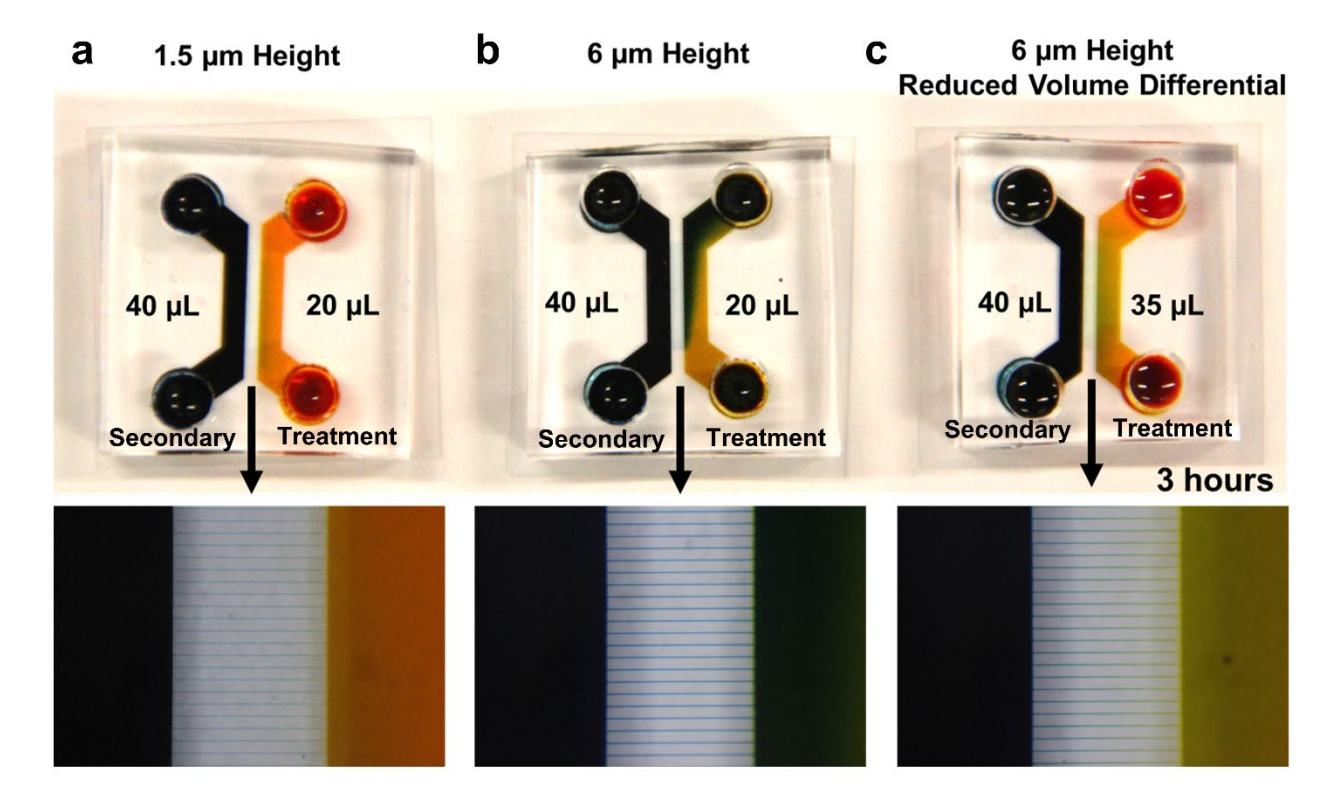


Figure S3: Comparing the fluid flow and fluidic isolation of different devices after 3 hours. In these devices a volume differential of 20 μL equated to a height differential of ~2.83 mm, while a volume differential of 5 μL equated to a height differential of ~0.71 mm. (a) For 1.5 μm height devices with a 20 μL volume differential we see both good fluidic isolation (negligible diffusive transport) and minimal flow between the chambers. (b) For the 6 μm height device and 20 μL volume differential there was good fluidic isolation, but significant flow between the chambers. (c) When the volume differential was reduced, the flow between the chambers was also reduced, but some of the dye from the isolated chamber (yellow) can be seen diffusing into the microchannels.

Supplemental Methods: Analytical and Computational Models.

The analytical model was based on the "full" style device with 101 microchannels with a channel length of 1000 μ m and a channel width of 10 μ m. The following electric circuit analogy with the four wells modeled as capacitors (C1-C4) and the interconnecting microchannels modeled as resistors (MC1-MC101).

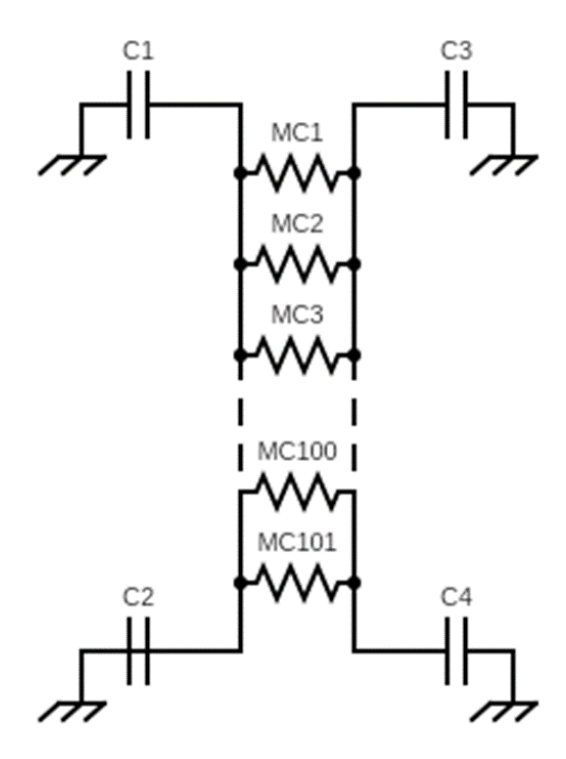


Figure S4: Electric circuit analogy used to estimate the fluid flow through the microchannels.

The change in volume between the chambers over time can be found using the following equation

$$V(t) = \frac{\Delta V}{2} \left(1 - e^{-\frac{2t}{RC}} \right)$$

Where ΔV is the initial volume differential between the chamber, R is the hydraulic resistance through the microchannels, and C is the "capacitance" of the wells. The hydraulic resistance through rectangular microchannels can be estimated using the following equation

$$R_H = \frac{12\mu L}{wh^3 \left(1 - 0.630 \left[\frac{h}{w}\right]\right)}$$

Where w, L, and h are the width, length, and height of the microchannel respectively, and μ is the dynamic viscosity. C is defined as the change in stored volumetric flow rate due to change in pressure and can be calculated for an open well as

$$C = \frac{\Delta V}{\Delta P} \propto Area_{Well}$$

Computational modeling was done in COMSOL Multiphysics 5.5 solving for the Navier-Stokes equations to model the pressure driven flow through the microchannels in a full 3D model of the "full" device with the following geometry: Chamber height: 75 μ m, Channel length: 1000 μ m, Channel width: 10 μ m, Channel height: variable, 101 channels.

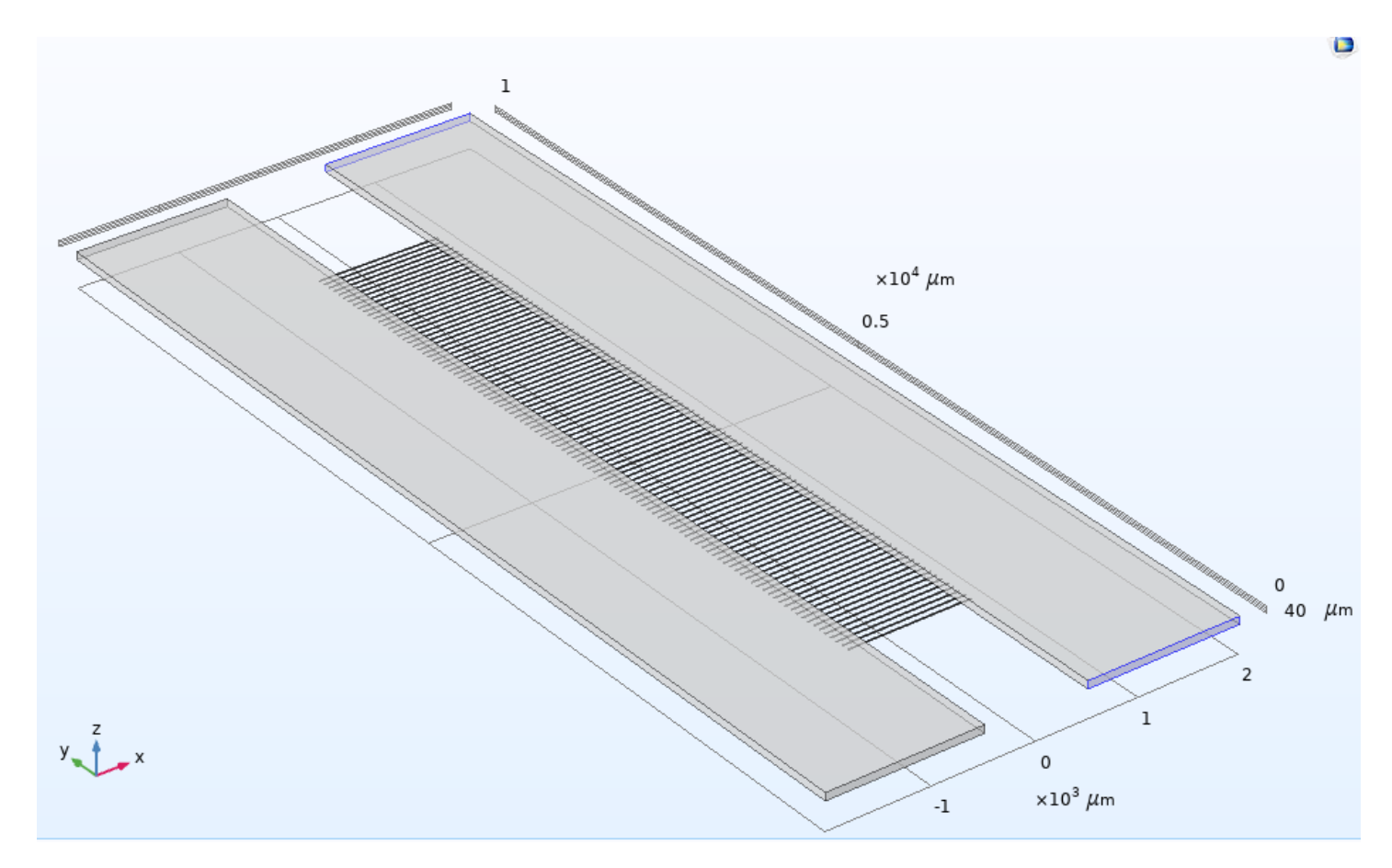


Figure S5: 3D geometry of the COMSOL model

The boundary conditions were set as follows: Inflow (Blue) with a set pressure equal to the volume differential of $150~\mu L$ per chamber ($75~\mu L$ per well), Outflow (opposing "openings"), No Flux (all other surfaces). The model was solved for steady state, and the volumetric flow rate was determined by taking the average velocity at the outflow multiplied by the surface area of the outflow boundaries.

References:

1. Goshi, Noah, Rhianna K. Morgan, Pamela J. Lein, and Erkin Seker. "A primary neural cell culture model to study neuron, astrocyte, and microglia interactions in neuroinflammation." Journal of neuroinflammation 17, no. 1 (2020): 1-16.

References Used for Figure S1 – Analysis of Microchannel Dimensions in Literature

- Brofiga, Martina; Pisano, Marietta; Tedesco, Mariateresa; Raiteri, Roberto; Massobrio, Paolo. "Three-dimensionality shapes the dynamics of cortical interconnected to hippocampal networks" JOURNAL OF NEURAL ENGINEERING (2020)
- 2. Katsikoudi, Antigoni; Ficulle, Elena; Cavallini, Annalisa; Sharman, Gary; Guyot, Amelie; Zagnoni, Michele; Eastwood, Brian J.; Hutton, Michael; Bose, Suchira. "Quantitative propagation of assembled human Tau from Alzheimer's disease brain in microfluidic neuronal cultures" JOURNAL OF BIOLOGICAL CHEMISTRY (2020)
- 3. Mazzara, Pietro Giuseppe; Muggeo, Sharon; Luoni, Mirko; Massimino, Luca; Zaghi, Mattia; Valverde, Parisa Tajalli-Tehrani; Brusco, Simone; Marzi, Matteo Jacopo; Palma, Cecilia; Colasante, Gaia; Iannielli, Angelo; Paulis, Marianna; Cordiglieri, Chiara; Giannelli, Serena Gea; Podini, Paola; Gellera, Cinzia; Taroni, Franco; Nicassio, Francesco; Rasponi, Marco; Broccoli, Vania. "Frataxin gene editing rescues Friedreich's ataxia pathology in dorsal root ganglia organoid-derived sensory neurons" NATURE COMMUNICATIONS (2020)
- 4. Bastiaens, Alex; Sabahi-Kaviani, Rahman; Luttge, Regina. "Nanogrooves for 2D and 3D Microenvironments of SH-SY5Y Cultures in Brain-on-Chip Technology" FRONTIERS IN NEUROSCIENCE (2020)

- Watters, Orla; Connolly, Niamh M. C.; Konig, Hans-Georg; Dussmann, Heiko; Prehn, Jochen H. M.. "AMPK Preferentially Depresses Retrograde Transport of Axonal Mitochondria during Localized Nutrient Deprivation" JOURNAL OF NEUROSCIENCE (2020)
- 6. Takayama, Yuzo; Kushige, Hiroko; Akagi, Yuka; Suzuki, Yutaka; Kumagai, Yutaro; Kida, Yasuyuki S.. "Selective Induction of Human Autonomic Neurons Enables Precise Control of Cardiomyocyte Beating" SCIENTIFIC REPORTS (2020)
- 7. Bruyere, Julie; Abada, Yah-Se; Vitet, Helene; Fontaine, Gaelle; Deloulme, Jean-Christophe; Ces, Aurelia; Denarier, Eric; Pernet-Gallay, Karin; Andrieux, Annie; Humbert, Sandrine; Potier, Marie-Claude; Delatour, Benoit; Saudou, Frederic. "Presynaptic APP levels and synaptic homeostasis are regulated by Akt phosphorylation of huntingtin" ELIFE (2020)
- 8. Asselin, Laure; Alvarez, Jose Rivera; Heide, Solveig; Bonnet, Camille S.; Tilly, Peggy; Vitet, Helene; Weber, Chantal; Bacino, Carlos A.; Baranano, Kristin; Chassevent, Anna; Dameron, Amy; Faivre, Laurence; Hanchard, Neil A.; Mahida, Sonal; McWalter, Kirsty; Mignot, Cyril; Nava, Caroline; Rastetter, Agnes; Streff, Haley; Thauvin-Robinet, Christel; Weiss, Marjan M.; Zapata, Gladys; Zwijnenburg, Petra J. G.; Saudou, Frederic; Depienne, Christel; Golzio, Christelle; Heron, Delphine; Godin, Juliette D.. "Mutations in the KIF21B kinesin gene cause neurodevelopmental disorders through imbalanced canonical motor activity" NATURE COMMUNICATIONS (2020)
- Wang, Tong; Li, Wei; Martin, Sally; Papadopulos, Andreas; Joensuu, Merja; Liu, Chunxia; Jiang, Anmin; Shamsollahi, Golnoosh; Amor, Rumelo; Lanoue, Vanessa; Padmanabhan, Pranesh; Meunier, Frederic A.. "Radial contractility of actomyosin rings facilitates axonal trafficking and structural stability" JOURNAL OF CELL BIOLOGY (2020)
- Fujita, Yuki; Nakanishi, Toru; Ueno, Masaki; Itohara, Shigeyoshi; Yamashita, Toshihide. "Netrin-G1 Regulates Microglial Accumulation along Axons and Supports the Survival of Layer V Neurons in the Postnatal Mouse Brain" CELL REPORTS (2020)
- 11. Vahsen, Bjoern Friedhelm; Ribas, Vinicius Toledo; Sundermeyer, Jonas; Boecker, Alexander; Dambeck, Vivian; Lenz, Christof; Shomroni, Orr; Gomes, Lucas Caldi; Tatenhorst, Lars; Barski, Elisabeth; Roser, Anna-Elisa; Michel, Uwe; Urlaub, Henning; Salinas, Gabriela; Baehr, Mathias; Koch, Christoph; Lingor, Paul. "Inhibition of the autophagic protein ULK1 attenuates axonal degeneration in vitro and in vivo, enhances translation, and modulates splicing" CELL DEATH AND DIFFERENTIATION (2020)
- 12. Fantuzzo, Joseph A.; Robles, Denise A.; Mirabella, Vincent R.; Hart, Ronald P.; Pang, Zhiping P.; Zahn, Jeffrey D.. "Development of a high-throughput arrayed neural circuitry platform using human induced neurons for drug screening applications" LAB ON A CHIP (2020)
- 13. Liu, Jianan; Li, Fangyuan; Wang, Yi; Pan, Limin; Lin, Peihua; Zhang, Bo; Zheng, Yanrong; Xu, Yingwei; Liao, Hongwei; Ko, Giho; Fei, Fan; Xu, Cenglin; Du, Yang; Shin, Kwangsoo; Kim, Dokyoon; Jang, Sung-Soo; Chung, Hee Jung; Tian, He; Wang, Qi; Guo, Wei; Nam, Jwa-Min; Chen, Zhong; Hyeon, Taeghwan; Ling, Daishun. "A sensitive and specific nanosensor for monitoring extracellular potassium levels in the brain" NATURE NANOTECHNOLOGY (2020)
- 14. Lucci, Cristiano; Mesquita-Ribeiro, Raquel; Rathbone, Alex; Dajas-Bailador, Federico. "Spatiotemporal regulation of GSK3 beta levels by miRNA-26a controls axon development in cortical neurons" DEVELOPMENT (2020)
- 15. Sundaramoorthy, Vinod; Green, Diane; Locke, Kelly; O'Brien, Carmel M.; Dearnley, Megan; Bingham, John. "Novel role of SARM1 mediated axonal degeneration in the pathogenesis of rabies" PLOS PATHOGENS (2020)
- 16. Iannielli, Angelo; Ugolini, Giovanni Stefano; Cordiglieri, Chiara; Bido, Simone; Rubio, Alicia; Colasante, Gaia; Valtorta, Marco; Cabassi, Tommaso; Rasponi, Marco; Broccoli, Vania. "Reconstitution of the Human Nigro-striatal Pathway on-a-Chip Reveals OPA1-Dependent Mitochondrial Defects and Loss of Dopaminergic Synapses" CELL REPORTS (2019)
- 17. Shigeoka, Toshiaki; Koppers, Max; Wong, Hovy Ho-Wai; Lin, Julie Qiaojin; Cagnetta, Roberta; Dwivedy, Asha; Nascimento, Janaina de Freitas; van Tartwijk, Francesca W.; Strohl, Florian; Cioni, Jean-Michel; Schaeffer, Julia; Carrington, Mark; Kaminski, Clemens F.; Jung, Hosung; Harris, William A.; Holt, Christine E.. "On-Site Ribosome Remodeling by Locally Synthesized Ribosomal Proteins in Axons" CELL REPORTS (2019)
- 18. Singh, Tanya; Vazquez, Maribel. "Time-Dependent Addition of Neuronal and Schwann Cells Increase Myotube Viability and Length in an In Vitro Tri-culture Model of the Neuromuscular Junction" REGENERATIVE ENGINEERING AND TRANSLATIONAL MEDICINE (2019)
- 19. Bellmann, Jessica; Goswami, Ruchi Y.; Girardo, Salvatore; Rein, Nelly; Hosseinzadeh, Zohreh; Hicks, Michael R.; Busskamp, Volker; Pyle, April D.; Werner, Carsten; Sterneckert, Jared. "A customizable microfluidic platform for medium-throughput modeling of neuromuscular circuits" BIOMATERIALS (2019)
- 20. Hyvarinen, Tanja; Hagman, Sanna; Ristola, Mervi; Sukki, Lassi; Veijula, Katariina; Kreutzer, Joose; Kallio, Pasi; Narkilahti, Susanna. "Co-stimulation with IL-1 beta and TNF-alpha induces an inflammatory reactive astrocyte phenotype with neurosupportive characteristics in a human pluripotent stem cell model system" SCIENTIFIC REPORTS (2019)

- 21. Nagendran, Tharkika; Taylor, Anne Marion. "Unique Axon-to-Soma Signaling Pathways Mediate Dendritic Spine Loss and Hyper-Excitability Post-axotomy" FRONTIERS IN CELLULAR NEUROSCIENCE (2019)
- 22. Wenzel, Erin D.; Speidell, Andrew; Flowers, Sarah A.; Wu, Chengbiao; Avdoshina, Valeria; Mocchetti, Italo. "Histone deacetylase 6 inhibition rescues axonal transport impairments and prevents the neurotoxicity of HIV-1 envelope protein gp120" CELL DEATH & DISEASE (2019)
- 23. Vysokov, Nickolai; McMahon, Stephen B.; Raouf, Ramin. "The role of Na-V channels in synaptic transmission after axotomy in a microfluidic culture platform" SCIENTIFIC REPORTS (2019)
- Lee, Soyeon; Wang, Wei; Hwang, Jinyeon; Namgung, Uk; Min, Kyung-Tai. "Increased ER-mitochondria tethering promotes axon regeneration" PROCEEDINGS OF THE NATIONAL ACADEMY OF SCIENCES OF THE UNITED STATES OF AMERICA (2019)
- Hixon, Alison M.; Clarke, Penny; Tyler, Kenneth L.. "Contemporary Circulating Enterovirus D68 Strains Infect and Undergo Retrograde Axonal Transport in Spinal Motor Neurons Independent of Sialic Acid" JOURNAL OF VIROLOGY (2019)
- 26. Costa, Rui O.; Martins, Helena; Martins, Luis F.; Cwetsch, Andrzej W.; Mele, Miranda; Pedro, Joana R.; Tome, Diogo; Jeon, Noo Li; Cancedda, Laura; Jaffrey, Samie R.; Almeida, Ramiro D.. "Synaptogenesis Stimulates a Proteasome-Mediated Ribosome Reduction in Axons" CELL REPORTS (2019)
- 27. Kamudzandu, M.; Kose-Dunn, M.; Evans, M. G.; Pricker, R. A.; Roach, P.. "A micro-fabricated in vitro complex neuronal circuit platform" BIOMEDICAL PHYSICS & ENGINEERING EXPRESS (2019)
- Vaquie, Adrien; Sauvain, Alizee; Duman, Mert; Nocera, Gianluigi; Egger, Boris; Meyenhofer, Felix; Falquet, Laurent; Bartesaghi, Luca; Chrast, Roman; Lamy, Christophe Maurice; Bang, Seokyoung; Lee, Seung-Ryeol; Li Jeon, Noo; Ruff, Sophie; Jacob, Claire. "Injured Axons Instruct Schwann Cells to Build Constricting Actin Spheres to Accelerate Axonal Disintegration" CELL REPORTS (2019)
- 29. Dixon, Angela R.; Horst, Eric N.; Garcia, Jeniffer J.; Ndjouyep-Yamaga, Patricia R.; Mehta, Geeta. "Morphometric and computational assessments to evaluate neuron survival and maturation within compartmentalized microfluidic devices: The influence of design variation on diffusion-driven nutrient transport" NEUROSCIENCE LETTERS (2019)
- 30. Zheng, Yanrong; Zhang, Xiangnan; Wu, Xiaoli; Jiang, Lei; Ahsan, Anil; Ma, Shijia; Xiao, Ziyu; Han, Feng; Qin, Zheng-Hong; Hu, Weiwei; Chen, Zhong. "Somatic autophagy of axonal mitochondria in ischemic neurons" JOURNAL OF CELL BIOLOGY (2019)
- 31. Ristola, Mervi; Sukki, Lassi; Azevedo, Maria Manuela; Seixas, Ana Isabel; Relvas, Joao Bettencourt; Narkilahti, Susanna; Kallio, Pasi. "A compartmentalized neuron-oligodendrocyte co-culture device for myelin research: design, fabrication and functionality testing" JOURNAL OF MICROMECHANICS AND MICROENGINEERING (2019)
- 32. Kamande, Joyce W.; Nagendran, Tharkika; Harris, Joseph; Taylor, Anne Marion. "Multi-compartment Microfluidic Device Geometry and Covalently Bound Poly-D-Lysine Influence Neuronal Maturation" FRONTIERS IN BIOENGINEERING AND BIOTECHNOLOGY (2019)
- 33. Yokoyama, S.; Otomo, A.; Hadano, S.; Kimura, H.. "An open-type microdevice to improve the quality of fluorescence labeling for axonal transport analysis in neurons" BIOMICROFLUIDICS (2019)
- 34. Pu, Hongjian; Shi, Yejie; Zhang, Lili; Lu, Zhengyu; Ye, Qing; Leak, Rehana K.; Xu, Fei; Ma, Shubei; Mu, Hongfeng; Wei, Zhishuo; Xu, Na; Xia, Yuguo; Hu, Xiaoming; Hitchens, T. Kevin; Bennett, Michael V. L.; Chen, Jun. "Protease-independent action of tissue plasminogen activator in brain plasticity and neurological recovery after ischemic stroke" PROCEEDINGS OF THE NATIONAL ACADEMY OF SCIENCES OF THE UNITED STATES OF AMERICA (2019)
- 35. Li, Chao; Zhang, Yi; Levin, Albert M.; Fan, Bao Yan; Teng, Hua; Ghannam, Moleca M.; Chopp, Michael; Zhang, Zheng Gang. "Distal Axonal Proteins and Their Related MiRNAs in Cultured Cortical Neurons" MOLECULAR NEUROBIOLOGY (2019)
- 36. Goto-Silva, Livia; McShane, Marisa P.; Salinas, Sara; Kalaidzidis, Yannis; Schiavo, Giampietro; Zerial, Marino. "Retrograde transport of Akt by a neuronal Rab5-APPL1 endosome" SCIENTIFIC REPORTS (2019)
- 37. Klim, Joseph R.; Williams, Luis A.; Limone, Francesco; San Juan, Irune Guerra; Davis-Dusenbery, Brandi N.; Mordes, Daniel A.; Burberry, Aaron; Steinbaugh, Michael J.; Gamage, Kanchana K.; Kirchner, Rory; Moccia, Rob; Casse, Seth H.; Chen, Kuchuan; Wainger, Brian J.; Woolf, Clifford J.; Eggan, Kevin. "ALS-implicated protein TDP-43 sustains levels of STMN2, a mediator of motor neuron growth and repair" NATURE NEUROSCIENCE (2019)
- 38. Melamed, Ze'ev; Lopez-Erauskin, Jone; Baughn, Michael W.; Zhang, Ouyang; Drenner, Kevin; YingSun; Freyermuth, Fernande; McMahons, Moira A.; Beccari, Melinda S.; Artates, Jon W.; Ohkubo, Takuya; Rodriguez, Maria; Lin, Nianwei; Wu, Dongmei; Bennetts, C. Frank; Rigos, Frank; Da Cruz, Sandrine; Ravits, John; Lagier-Tourenne, Clotilde; Cleveland, Don W.. "Premature polyadenylation-mediated loss of stathmin-2 is a hallmark of TDP-43-dependent neurodegeneration" NATURE NEUROSCIENCE (2019)
- 39. Lesniak, Anna; Kilinc, Devrim; Blasiak, Agata; Galea, George; Simpson, Jeremy C.; Lee, Gil U.. "Rapid Growth Cone Uptake and Dynein-Mediated Axonal Retrograde Transport of Negatively Charged Nanoparticles in Neurons Is Dependent on Size and Cell Type" SMALL (2019)

- 40. Nijssen, Jik; Aguila, Julio; Hoogstraaten, Rein; Kee, Nigel; Hedlund, Eva. "Axon-Seq Decodes the Motor Axon Transcriptome and Its Modulation in Response to ALS" STEM CELL REPORTS (2018)
- Balaji, Varun; Kaniyappan, Senthilvelrajan; Mandelkow, Eckhard; Wang, Yipeng; Mandelkow, Eva-Maria.
 "Pathological missorting of endogenous MAPT/Tau in neurons caused by failure of protein degradation systems" AUTOPHAGY (2018)
- 42. Jia, Longfei; Chopp, Michael; Wang, Lei; Lu, Xuerong; Szalad, Alexandra; Zhang, Zheng Gang. "Exosomes derived from high-glucose-stimulated Schwann cells promote development of diabetic peripheral neuropathy" FASEB JOURNAL (2018)
- 43. Jia, Longfei; Chopp, Michael; Wang, Lei; Lu, Xuerong; Zhang, Yi; Szalad, Alexandra; Zhang, Zheng Gang. "MiR-34a Regulates Axonal Growth of Dorsal Root Ganglia Neurons by Targeting FOXP2 and VAT1 in Postnatal and Adult Mouse" MOLECULAR NEUROBIOLOGY (2018)
- 44. Vysokov, Nickolai V.; Silva, John-Paul; Lelianova, Vera G.; Suckling, Jason; Cassidy, John; Blackburn, Jennifer K.; Yankova, Natalia; Djamgoz, Mustafa B. A.; Kozlov, Serguei V.; Tonevitsky, Alexander G.; Ushkaryov, Yuri A.. "Proteolytically released Lasso/teneurin-2 induces axonal attraction by interacting with latrophilin-1 on axonal growth cones" ELIFE (2018)
- 45. Wang, Ze Zhong; Wood, Matthew D.; Mackinnon, Susan E.; Sakiyama-Elbert, Shelly E.. "A microfluidic platform to study the effects of GDNF on neuronal axon entrapment" JOURNAL OF NEUROSCIENCE METHODS (2018)
- 46. Van Laar, Victor S.; Arnold, Beth; Howlett, Evan H.; Calderon, Michael J.; St Croix, Claudette M.; Greenamyre, J. Timothy; Sanders, Laurie H.; Berman, Sarah B.. "Evidence for Compartmentalized Axonal Mitochondrial Biogenesis: Mitochondrial DNA Replication Increases in Distal Axons As an Early Response to Parkinson's Disease-Relevant Stress" JOURNAL OF NEUROSCIENCE (2018)
- 47. Poli, Daniele; Wheeler, Bruce C.; DeMarse, Thomas B.; Brewer, Gregory J.. "Pattern separation and completion of distinct axonal inputs transmitted via micro-tunnels between co-cultured hippocampal dentate, CA3, CA1 and entorhinal cortex networks" JOURNAL OF NEURAL ENGINEERING (2018)
- 48. Clark, Alex J.; Menendez, Guillermo; AlQatari, Mona; Patel, Niral; Arstad, Erik; Schiavo, Giampietro; Koltzenburg, Martin. "Functional imaging in microfluidic chambers reveals sensory neuron sensitivity is differentially regulated between neuronal regions" PAIN (2018)
- 49. Jocher, Georg; Mannschatz, Sidney H.; Offterdinger, Martin; Schweigreiter, Ruediger. "Microfluidics of Small-Population Neurons Allows for a Precise Quantification of the Peripheral Axonal Growth State" FRONTIERS IN CELLULAR NEUROSCIENCE (2018)
- 50. Santhanam, Navaneetha; Kumanchik, Lee; Guo, Xiufang; Sommerhage, Frank; Cai, Yunqing; Jackson, Max; Martin, Candace; Saad, George; McAleer, Christopher W.; Wang, Ying; Lavado, Andrea; Long, Christopher J.; Hickman, James J.. "Stem cell derived phenotypic human neuromuscular junction model for dose response evaluation of therapeutics" BIOMATERIALS (2018)
- Urrea, Laura; Segura-Feliu, Miriam; Masuda-Suzukake, Masami; Hervera, Arnau; Pedraz, Lucas; Garcia Aznar, Jose Manuel; Vila, Miquel; Samitier, Josep; Torrents, Eduard; Ferrer, Isidro; Gavin, Rosalina; Hagesawa, Masato; Antonio del Rio, Jose. "Involvement of Cellular Prion Protein in alpha-Synuclein Transport in Neurons" MOLECULAR NEUROBIOLOGY (2018)
- 52. Polanco, Juan Carlos; Li, Chuanzhou; Durisic, Nela; Sullivan, Robert; Gotz, Jurgen. "Exosomes taken up by neurons hijack the endosomal pathway to spread to interconnected neurons" ACTA NEUROPATHOLOGICA COMMUNICATIONS (2018)
- 53. Clarkson, Benjamin D. S.; Patel, Misha S.; LaFrance-Corey, Reghann G.; Howe, Charles L.. "Retrograde interferongamma signaling induces major histocompatibility class I expression in human-induced pluripotent stem cell-derived neurons" ANNALS OF CLINICAL AND TRANSLATIONAL NEUROLOGY (2018)
- 54. Virlogeux, Amandine; Moutaux, Eve; Christaller, Wilhelm; Genoux, Aurelie; Bruyere, Julie; Fino, Elodie; Charlot, Benoit; Cazorla, Maxime; Saudou, Frederic. "Reconstituting Corticostriatal Network on-a-Chip Reveals the Contribution of the Presynaptic Compartment to Huntington's Disease" CELL REPORTS (2018)
- van de Wijdeven, Rosanne; Ramstad, Ola Huse; Bauer, Ulrich Stefan; Halaas, Oyvind; Sandvig, Axel; Sandvig, loanna. "Structuring a multi-nodal neural network in vitro within a novel design microfluidic chip" BIOMEDICAL MICRODEVICES (2018)
- 56. Mills, Richard; Taylor-Weiner, Hermes; Correia, Jorge C.; Agudelo, Leandro Z.; Allodi, Ilary; Kolonelou, Christina; Martinez-Redondo, Vicente; Ferreira, Duarte M. S.; Nichterwitz, Susanne; Comley, Laura H.; Lundin, Vanessa; Hedlund, Eva; Ruas, Jorge L.; Teixeira, Ana I.. "Neurturin is a PGC-1 alpha 1-controlled myokine that promotes motor neuron recruitment and neuromuscular junction formation" MOLECULAR METABOLISM (2018)
- Jia, Longfei; Wang, Lei; Chopp, Michael; Li, Chao; Zhang, Yi; Szalad, Alexandra; Zhang, Zheng Gang. "MiR-29c/PRKCI Regulates Axonal Growth of Dorsal Root Ganglia Neurons Under Hyperglycemia" MOLECULAR NEUROBIOLOGY (2018)

- 58. Sun, Tao; Li, Yuan; Li, Ting; Ma, Huixian; Guo, Yunyun; Jiang, Xingyu; Hou, Ming; Huang, Shuhong; Chen, Zheyu. "JIP1 and JIP3 cooperate to mediate TrkB anterograde axonal transport by activating kinesin-1" CELLULAR AND MOLECULAR LIFE SCIENCES (2017)
- 59. Bauer, Dirk; Alt, Mira; Dirks, Miriam; Buch, Anna; Heilingloh, Christiane S.; Dittmer, Ulf; Giebel, Bernd; Goergens, Andre; Palapys, Vivien; Kasper, Maren; Eis-Huebinger, Anna M.; Sodeik, Beate; Heiligenhaus, Arnd; Roggendorf, Michael; Krawczyk, Adalbert. "A Therapeutic Antiviral Antibody Inhibits the Anterograde Directed Neuron-to-Cell Spread of Herpes Simplex Virus and Protects against Ocular Disease" FRONTIERS IN MICROBIOLOGY (2017)
- 60. Nagendran, Tharkika; Larsen, Rylan S.; Bigler, Rebecca L.; Frost, Shawn B.; Philpot, Benjamin D.; Nudo, Randolph J.; Taylor, Anne Marion. "Distal axotomy enhances retrograde presynaptic excitability onto injured pyramidal neurons via trans-synaptic signaling" NATURE COMMUNICATIONS (2017)
- 61. Habibey, Rouhollah; Latifi, Shahrzad; Mousavi, Hossein; Pesce, Mattia; Arab-Tehrany, Elmira; Blau, Axel. "A multielectrode array microchannel platform reveals both transient and slow changes in axonal conduction velocity" SCIENTIFIC REPORTS (2017)
- 62. Sakai, Koji; Shimba, Kenta; Kotani, Kiyoshi; Jimbo, Yasuhiko. "A co-culture microtunnel technique demonstrating a significant contribution of unmyelinated Schwann cells to the acceleration of axonal conduction in Schwann cell-regulated peripheral nerve development" INTEGRATIVE BIOLOGY (2017)
- 63. Peikon, Ian D.; Kebschull, Justus M.; Vagin, Vasily V.; Ravens, Diana I.; Sun, Yu-Chi; Brouzes, Eric; Correa, Ivan R., Jr.; Bressan, Dario; Zador, Anthony M.. "Using high-throughput barcode sequencing to efficiently map connectomes" NUCLEIC ACIDS RESEARCH (2017)
- 64. Martins, Lus F.; Costa, Rui O.; Pedro, Joana R.; Aguiar, Paulo; Serra, Sofia C.; Teixeira, Fabio G.; Sousa, Nuno; Salgado, Antonio J.; Almeida, Ramiro D.. "Mesenchymal stem cells secretome-induced axonal outgrowth is mediated by BDNF" SCIENTIFIC REPORTS (2017)
- 65. Jiang, Hai-Fei; Wang, Wei; Jiang, Xuan; Zeng, Wen-Bo; Shen, Zhang-Zhou; Song, Yi-Ge; Yang, Hong; Liu, Xi-Juan; Dong, Xiao; Zhou, Jing; Sun, Jin-Yan; Yu, Fei-Long; Guo, Lin; Cheng, Tong; Rayner, Simon; Zhao, Fei; Zhu, Hua; Luo, Min-Hua. "ORF7 of Varicella-Zoster Virus Is Required for Viral Cytoplasmic Envelopment in Differentiated Neuronal Cells" JOURNAL OF VIROLOGY (2017)
- 66. Zeng, Wen-Bo; Jiang, Hai-Fei; Gang, Ya-Dong; Song, Yi-Ge; Shen, Zhang-Zhou; Yang, Hong; Dong, Xiao; Tian, Yong-Lu; Ni, Rong-Jun; Liu, Yaping; Tang, Na; Li, Xinyan; Jiang, Xuan; Gao, Ding; Androulakis, Michelle; He, Xiao-Bin; Xia, Hui-Min; Ming, Ying-Zi; Lu, Youming; Zhou, Jiang-Ning; Zhang, Chen; Xia, Xue-Shan; Shu, Yousheng; Zeng, Shao-Qun; Xu, Fuqiang; Zhao, Fei; Luo, Min-Hua. "Anterograde monosynaptic transneuronal tracers derived from herpes simplex virus 1 strain H129" MOLECULAR NEURODEGENERATION (2017)
- 67. Narula, Udit; Ruiz, Andres; McQuaide, McKinley; DeMarse, Thomas B.; Wheeler, Bruce C.; Brewer, Gregory J.. "Narrow microtunnel technology for the isolation and precise identification of axonal communication among distinct hippocampal subregion networks" PLOS ONE (2017)
- 68. Yap, Yiing C.; King, Anna E.; Guijt, Rosanne M.; Jiang, Tongcui; Blizzard, Catherine A.; Breadmore, Michael C.; Dickson, Tracey C.. "Mild and repetitive very mild axonal stretch injury triggers cystoskeletal mislocalization and growth cone collapse" PLOS ONE (2017)
- 69. Zhang, Yi; Chopp, Michael; Liu, Xian Shuang; Katakowski, Mark; Wang, Xinli; Tian, Xinchu; Wu, David; Zhang, Zheng Gang. "Exosomes Derived from Mesenchymal Stromal Cells Promote Axonal Growth of Cortical Neurons" MOLECULAR NEUROBIOLOGY (2017)
- Suzuki, Koji; Tanaka, Hiroyuki; Ebara, Mitsuhiro; Uto, Koichiro; Matsuoka, Hozo; Nishimoto, Shunsuke; Okada, Kiyoshi; Murase, Tsuyoshi; Yoshikawa, Hideki. "Electrospun nanofiber sheets incorporating methylcobalamin promote nerve regeneration and functional recovery in a rat sciatic nerve crush injury model" ACTA BIOMATERIALIA (2017)
- 71. Li, Wei; Xu, Zhen; Xu, Bingzhe; Chan, Chung Yuen; Lin, Xudong; Wang, Ying; Chen, Ganchao; Wang, Zhigang; Yuan, Qiuju; Zhu, Guangyu; Sun, Hongyan; Wu, Wutian; Shi, Peng. "Investigation of the Subcellular Neurotoxicity of Amyloid-beta Using a Device Integrating Microfluidic Perfusion and Chemotactic Guidance" ADVANCED HEALTHCARE MATERIALS (2017)
- 72. Bigler, Rebecca L.; Kamande, Joyce W.; Dumitru, Raluca; Niedringhaus, Mark; Taylor, Anne Marion. "Messenger RNAs localized to distal projections of human stem cell derived neurons" SCIENTIFIC REPORTS (2017)
- Lombardi, Loredana; Persiconi, Irene; Gallo, Alessandra; Hoogenraad, Casper C.; De Stefano, Maria Egle. "NGFdependent axon growth and regeneration are altered in sympathetic neurons of dystrophic mdx mice" MOLECULAR AND CELLULAR NEUROSCIENCE (2017)
- 74. Hong, Nari; Joo, Sunghoon; Nam, Yoonkey. "Characterization of Axonal Spikes in Cultured Neuronal Networks Using Microelectrode Arrays and Microchannel Devices" IEEE TRANSACTIONS ON BIOMEDICAL ENGINEERING (2017)

- 75. Shimba, Kenta; Sakai, Koji; Kotani, Kiyoshi; Yagi, Tohru; Jimbo, Yasuhiko. "Microtunnel-Electrode Device for Elucidating Axon Features: toward Pharmacological Manipulation of Individual Axons" 2017 8TH INTERNATIONAL IEEE/EMBS CONFERENCE ON NEURAL ENGINEERING (NER) (2017)
- 76. Cui, Chengcheng; Ye, Xinchun; Chopp, Michael; Venkat, Poornima; Zacharek, Alex; Yan, Tao; Ning, Ruizhou; Yu, Peng; Cui, Guiyun; Chen, Jieli. "miR-145 Regulates Diabetes-Bone Marrow Stromal Cell-Induced Neurorestorative Effects in Diabetes Stroke Rats" STEM CELLS TRANSLATIONAL MEDICINE (2016)
- 77. Yan, Tao; Venkat, Poornima; Chopp, Michael; Zacharek, Alex; Ning, Ruizhuo; Roberts, Cynthia; Zhang, Yi; Lu, Mei; Chen, Jieli. "Neurorestorative Responses to Delayed Human Mesenchymal Stromal Cells Treatment of Stroke in Type 2 Diabetic Rats" STROKE (2016)
- 78. Wang, Tong; Martin, Sally; Nguyen, Tam H.; Harper, Callista B.; Gormal, Rachel S.; Martinez-Marmol, Ramon; Karunanithi, Shanker; Coulson, Elizabeth J.; Glass, Nick R.; Cooper-White, Justin J.; van Swinderen, Bruno; Meunier, Frederic A.. "Flux of signalling endosomes undergoing axonal retrograde transport is encoded by presynaptic activity and TrkB" NATURE COMMUNICATIONS (2016)
- 79. Bomba-Warczak, Ewa; Vevea, Jason D.; Brittain, Joel M.; Figueroa-Bernier, Annette; Tepp, William H.; Johnson, Eric A.; Yeh, Felix L.; Chapman, Edwin R.. "Interneuronal Transfer and Distal Action of Tetanus Toxin and Botulinum Neurotoxins A and D in Central Neurons" CELL REPORTS (2016)
- 80. Eitan, Erez; Petralia, Ronald S.; Wang, Ya-Xian; Indig, Fred E.; Mattson, Mark P.; Yao, Pamela J.. "Probing extracellular Sonic hedgehog in neurons" BIOLOGY OPEN (2016)
- 81. Chen, Meifan; Geoffroy, Cedric G.; Wong, Hetty N.; Tress, Oliver; Nguyen, Mallorie T.; Holzman, Lawrence B.; Jin, Yishi; Zheng, Binhai. "Leucine Zipper-bearing Kinase promotes axon growth in mammalian central nervous system neurons" SCIENTIFIC REPORTS (2016)
- 82. Jia, Longfei; Wang, Lei; Chopp, Michael; Zhang, Yi; Szalad, Alexandra; Zhang, Zheng Gang. "MicroRNA 146a LOCALLY MEDIATES DISTAL AXONAL GROWTH OF DORSAL ROOT GANGLIA NEURONS UNDER HIGH GLUCOSE AND SILDENAFIL CONDITIONS" NEUROSCIENCE (2016)
- 83. Kim, Hyun Soo; Jeong, Sehoon; Koo, Chiwan; Han, Arum; Park, Jaewon. "A Microchip for High-Throughput Axon Growth Drug Screening" MICROMACHINES (2016)
- 84. Piccinotti, Silvia; Whelan, Sean P. J.. "Rabies Internalizes into Primary Peripheral Neurons via Clathrin Coated Pits and Requires Fusion at the Cell Body" PLOS PATHOGENS (2016)
- 85. Carballo-Molina, Oscar A.; Sanchez-Navarro, Andrea; Lopez-Ornelas, Adolfo; Lara-Rodarte, Rolando; Salazar, Patricia; Campos-Romo, Aurelio; Ramos-Mejia, Veronica; Velasco, Ivan. "Semaphorin 3C Released from a Biocompatible Hydrogel Guides and Promotes Axonal Growth of Rodent and Human Dopaminergic Neurons" TISSUE ENGINEERING PART A (2016)
- 86. Kos, Aron; Wanke, Kai A.; Gioio, Anthony; Martens, Gerard J.; Kaplan, Barry B.; Aschrafi, Armaz. "Monitoring mRNA Translation in Neuronal Processes Using Fluorescent Non-Canonical Amino Acid Tagging" JOURNAL OF HISTOCHEMISTRY & CYTOCHEMISTRY (2016)
- 87. DeMarse, Thomas B.; Pan, Liangbin; Alagapan, Sankaraleengam; Brewer, GregoryJ.; Wheeler, Bruce C.. "Feed-Forward Propagation of Temporal and Rate Information between Cortical Populations during Coherent Activation in Engineered In Vitro Networks" FRONTIERS IN NEURAL CIRCUITS (2016)
- 88. Brahic, Michel; Bousset, Luc; Bieri, Gregor; Melki, Ronald; Gitler, Aaron D.. "Axonal transport and secretion of fibrillar forms of alpha-synuclein, A beta 42 peptide and HTTExon 1" ACTA NEUROPATHOLOGICA (2016)
- 89. Lewandowska, Marta K.; Radivojevic, Milos; Jaeckel, David; Mueller, Jan; Hierlemann, Andreas R.. "Cortical Axons, Isolated in Channels, Display Activity-Dependent Signal Modulation as a Result of Targeted Stimulation" FRONTIERS IN NEUROSCIENCE (2016)
- 90. Gao, Yandong; Broussard, Joey; Haque, Amranul; Revzin, Alexander; Lin, Tian. "Functional imaging of neuron-astrocyte interactions in a compartmentalized microfluidic device" MICROSYSTEMS & NANOENGINEERING (2016)
- 91. Takayama, Yuzo; Kida, Yasuyuki S.. "In Vitro Reconstruction of Neuronal Networks Derived from Human iPS Cells Using Microfabricated Devices" PLOS ONE (2016)
- 92. Ionescu, Ariel; Zahavi, Eitan Erez; Gradus, Tal; Ben-Yaakov, Keren; Perlson, Eran. "Compartmental microfluidic system for studying muscle-neuron communication and neuromuscular junction maintenance" EUROPEAN JOURNAL OF CELL BIOLOGY (2016)
- 93. Uryu, Daiki; Tamaru, Tomohiro; Suzuki, Azusa; Sakai, Rie; Konishi, Yoshiyuki. "Study of local intracellular signals regulating axonal morphogenesis using a microfluidic device" SCIENCE AND TECHNOLOGY OF ADVANCED MATERIALS (2016)
- 94. Lei, Yifeng; Li, Jun; Wang, Nuoxin; Yang, Xinglong; Hamada, Yoh; Li, Qizhai; Zheng, Wenfu; Jiang, Xingyu. "An on-chip model for investigating the interaction between neurons and cancer cells" INTEGRATIVE BIOLOGY (2016)
- 95. Chen, Jieli; Ning, Ruizhuo; Zacharek, Alex; Cui, Chengcheng; Cui, Xu; Yan, Tao; Venkat, Poornima; Zhang, Yi; Chopp, Michael. "MiR-126 Contributes to Human Umbilical Cord Blood Cell-Induced Neurorestorative Effects After Stroke in Type-2 Diabetic Mice" STEM CELLS (2016)

- 96. Yao, Pamela J.; Petralia, Ronald S.; Ott, Carolyn; Wang, Ya-Xian; Lippincott-Schwartz, Jennifer; Mattson, Mark P.. "Dendrosomatic Sonic Hedgehog Signaling in Hippocampal Neurons Regulates Axon Elongation" JOURNAL OF NEUROSCIENCE (2015)
- 97. Isomura, Takuya; Shimba, Kenta; Takayama, Yuzo; Takeuchi, Akimasa; Kotani, Kiyoshi; Jimbo, Yasuhiko. "Signal transfer within a cultured asymmetric cortical neuron circuit" JOURNAL OF NEURAL ENGINEERING (2015)
- 98. Mika, Johann K.; Schwarz, Karin; Wanzenboeck, Heinz D.; Scholze, Petra; Bertagnolli, Emmerich. "Investigation of Neurotrophic Factor Concentrations with a Novel In Vitro Concept for Peripheral Nerve Regeneration" JOURNAL OF NEUROSCIENCE RESEARCH (2015)
- 99. Usenovic, Marija; Niroomand, Shahriar; Drolet, Robert E.; Yao, Lihang; Gaspar, Renee C.; Hatcher, Nathan G.; Schachter, Joel; Renger, John J.; Parmentier-Batteur, Sophie. "Internalized Tau Oligomers Cause Neurodegeneration by Inducing Accumulation of Pathogenic Tau in Human Neurons Derived from Induced Pluripotent Stem Cells" JOURNAL OF NEUROSCIENCE (2015)
- 100. Takeda, Shuko; Wegmann, Susanne; Cho, Hansang; Devos, Sarah L.; Commins, Caitlin; Roe, Allyson D.; Nicholls, Samantha B.; Carlson, George A.; Pitstick, Rose; Nobuhara, Chloe K.; Costantino, Isabel; Frosch, Matthew P.; Mueller, Daniel J.; Irimia, Daniel; Hyman, Bradley T.. "Neuronal uptake and propagation of a rare phosphorylated high-molecular-weight tau derived from Alzheimer's disease brain" NATURE COMMUNICATIONS (2015)
- 101. Li, Yu-Tao; Zhang, Shu-Hui; Wang, Xue-Ying; Zhang, Xin-Wei; Oleinick, Alexander I.; Svir, Irina; Amatore, Christian; Huang, Wei-Hua. "Real-time Monitoring of Discrete Synaptic Release Events and Excitatory Potentials within Self-reconstructed Neuromuscular Junctions" ANGEWANDTE CHEMIE-INTERNATIONAL EDITION (2015)
- 102. Lin, Shen; Nazif, Kutaiba; Smith, Alexander; Baas, Peter W.; Smith, George M.. "Histone acetylation inhibitors promote axon growth in adult dorsal root ganglia neurons" JOURNAL OF NEUROSCIENCE RESEARCH (2015)
- 103. Pan, Liangbin; Alagapan, Sankaraleengam; Franca, Eric; Leondopulos, Stathis S.; DeMarse, Thomas B.; Brewer, Gregory J.; Wheeler, Bruce C.. "An in vitro method to manipulate the direction and functional strength between neural populations" FRONTIERS IN NEURAL CIRCUITS (2015)
- 104. Reginensi, Diego; Carulla, Patricia; Nocentini, Sara; Seira, Oscar; Serra-Picamal, Xavier; Torres-Espin, Abel; Matamoros-Angles, Andreu; Gavin, Rosalina; Teresa Moreno-Flores, Maria; Wandosell, Francisco; Samitier, Josep; Trepat, Xavier; Navarro, Xavier; Antonio del Rio, Jose. "Increased migration of olfactory ensheathing cells secreting the Nogo receptor ectodomain over inhibitory substrates and lesioned spinal cord" CELLULAR AND MOLECULAR LIFE SCIENCES (2015)
- 105. Kerman, Bilal E.; Kim, Hyung Joon; Padmanabhan, Krishnan; Mei, Arianna; Georges, Shereen; Joens, Matthew S.; Fitzpatrick, James A. J.; Jappelli, Roberto; Chandross, Karen J.; August, Paul; Gage, Fred H.. "In vitro myelin formation using embryonic stem cells" DEVELOPMENT (2015)
- 106. Markus, Amos; Lebenthal-Loinger, Ilana; Yang, In Hong; Kinchington, Paul R.; Goldstein, Ronald S.. "An In Vitro Model of Latency and Reactivation of Varicella Zoster Virus in Human Stem Cell-Derived Neurons" PLOS PATHOGENS (2015)
- 107. Calafate, Sara; Buist, Arjan; Miskiewicz, Katarzyna; Vijayan, Vinoy; Daneels, Guy; de Strooper, Bart; de Wit, Joris; Verstreken, Patrik; Moechars, Diederik. "Synaptic Contacts Enhance Cell-to-Cell Tau Pathology Propagation" CELL REPORTS (2015)
- 108. Renault, Renaud; Sukenik, Nirit; Descroix, Stephanie; Malaquin, Laurent; Viovy, Jean-Louis; Peyrin, Jean-Michel; Bottani, Samuel; Monceau, Pascal; Moses, Elisha; Vignes, Maeva. "Combining Microfluidics, Optogenetics and Calcium Imaging to Study Neuronal Communication In Vitro" PLOS ONE (2015)
- 109. Wang, Tong; Martin, Sally; Papadopulos, Andreas; Harper, Callista B.; Mavlyutov, Timur A.; Niranjan, Dhevahi; Glass, Nick R.; Cooper-White, Justin J.; Sibarita, Jean-Baptiste; Choquet, Daniel; Davletov, Bazbek; Meunier, Frederic A.. "Control of Autophagosome Axonal Retrograde Flux by Presynaptic Activity Unveiled Using Botulinum Neurotoxin Type A" JOURNAL OF NEUROSCIENCE (2015)
- 110. Deglincerti, Alessia; Liu, Yaobin; Colak, Dilek; Hengst, Ulrich; Xu, Guoqiang; Jaffrey, Samie R.. "Coupled local translation and degradation regulate growth cone collapse" NATURE COMMUNICATIONS (2015)
- 111. Dixon, Angela R.; Philbert, Martin A.. "Morphometric assessment of toxicant induced neuronal degeneration in full and restricted contact co-cultures of embryonic cortical rat neurons and astrocytes: Using m-Dinitrobezene as a model neurotoxicant" TOXICOLOGY IN VITRO (2015)
- 112. Speranza, Luisa; Giuliano, Teresa; Volpicelli, Floriana; De Stefano, M. Egle; Lombardi, Loredana; Chambery, Angela; Lacivita, Enza; Leopoldo, Marcello; Bellenchi, Gian C.; di Porzio, Umberto; Crispino, Marianna; Perrone-Capano, Carla. "Activation of 5-HT7 receptor stimulates neurite elongation through mTOR, Cdc42 and actin filaments dynamics" FRONTIERS IN BEHAVIORAL NEUROSCIENCE (2015)
- 113. Lewandowska, Marta K.; Bakkum, Douglas J.; Rompani, Santiago B.; Hierlemann, Andreas. "Recording Large Extracellular Spikes in Microchannels along Many Axonal Sites from Individual Neurons" PLOS ONE (2015)
- 114. Marquardt, Laura M.; Sakiyama-Elbert, Shelly E.. "GDNF preconditioning can overcome Schwann cell phenotypic memory" EXPERIMENTAL NEUROLOGY (2015)

- 115. Niederst, Emily D.; Reyna, Sol M.; Goldstein, Lawrence S. B.. "Axonal amyloid precursor protein and its fragments undergo somatodendritic endocytosis and processing" MOLECULAR BIOLOGY OF THE CELL (2015)
- 116. Sakai, Koji; Shimba, Kenta; Kotani, Kiyoshi; Jimbo, Yasuhiko. "Microfabricated multi-electrode device for detecting oligodendrocyte-regulated changes in axonal conduction velocity" 2015 37TH ANNUAL INTERNATIONAL CONFERENCE OF THE IEEE ENGINEERING IN MEDICINE AND BIOLOGY SOCIETY (EMBC) (2015)
- 117. Selfridge, Aaron; Hyun, Nicholas; Chiang, Chai-Chun; Reyna, Sol M.; Weissmiller, April M.; Shi, Linda Z.; Preece, Daryl; Mobley, William C.; Berns, Michael W.. "Rat embryonic hippocampus and induced pluripotent stem cell derived cultured neurons recover from laser-induced subaxotomy" NEUROPHOTONICS (2015)
- 118. Habibey, Rouhollah; Golabchi, Asiyeh; Latifi, Shahrzad; Difato, Francesco; Blau, Axel. "A microchannel device tailored to laser axotomy and long-term microelectrode array electrophysiology of functional regeneration" LAB ON A CHIP (2015)
- 119. Chiang, Hao; Ohno, Nobuhiko; Hsieh, Yu-Lin; Mahad, Don J.; Kikuchi, Shin; Komuro, Hitoshi; Hsieh, Sung-Tsang; Trapp, Bruce D.. "Mitochondrial fission augments capsaicin-induced axonal degeneration" ACTA NEUROPATHOLOGICA (2015)
- 120. Tong, Ziqiu; Segura-Feliu, Miriam; Seira, Oscar; Homs-Corbera, Antoni; Antonio Del Rio, Jose; Samitier, Josep. "A microfluidic neuronal platform for neuron axotomy and controlled regenerative studies" RSC ADVANCES (2015)
- 121. Ashrafi, Ghazaleh; Schlehe, Julia S.; LaVoie, Matthew J.; Schwarz, Thomas L.. "Mitophagy of damaged mitochondria occurs locally in distal neuronal axons and requires PINK1 and Parkin" JOURNAL OF CELL BIOLOGY (2014)
- 122. Wu, Kong-Yan; He, Miao; Hou, Qiong-Qiong; Sheng, Ai-Li; Yuan, Lei; Liu, Fei; Liu, Wen-Wen; Li, Guangpu; Jiang, Xing-Yu; Luo, Zhen-Ge. "Semaphorin 3A activates the guanosine triphosphatase Rab5 to promote growth cone collapse and organize callosal axon projections" SCIENCE SIGNALING (2014)
- 123. Gluska, Shani; Zahavi, Eitan Erez; Chein, Michael; Gradus, Tal; Bauer, Anja; Finke, Stefan; Perlson, Eran. "Rabies Virus Hijacks and Accelerates the p75NTR Retrograde Axonal Transport Machinery" PLOS PATHOGENS (2014)
- 124. Yap, Yiing C.; Dickson, Tracey C.; King, Anna E.; Breadmore, Michael C.; Guijt, Rosanne M.. "Microfluidic culture platform for studying neuronal response to mild to very mild axonal stretch injuryn" BIOMICROFLUIDICS (2014)
- 125. Tran, Hien T.; Chung, Charlotte Hiu-Yan; Iba, Michiyo; Zhang, Bin; Trojanowski, John Q.; Luk, Kelvin C.; Lee, Virginia M. Y.. "alpha-Synuclein Immunotherapy Blocks Uptake and Templated Propagation of Misfolded alpha-Synuclein and Neurodegeneration" CELL REPORTS (2014)
- 126. Pan, Liangbin; Alagapan, Sankaraleengam; Franca, Eric; DeMarse, Thomas; Brewer, Gregory J.; Wheeler, Bruce C.. "Large Extracellular Spikes Recordable From Axons in Microtunnels" IEEE TRANSACTIONS ON NEURAL SYSTEMS AND REHABILITATION ENGINEERING (2014)
- 127. Otsmane, Belkacem; Moumen, Anice; Aebischer, Julianne; Coque, Emmanuelle; Sar, Chamroeun; Sunyach, Claire; Salsac, Celine; Valmier, Jean; Salinas, Sara; Bowerman, Melissa; Raoul, Cedric. "Somatic and axonal LIGHT signaling elicit degenerative and regenerative responses in motoneurons, respectively" EMBO REPORTS (2014)
- 128. Brewer, Bryson M.; Shi, Mingjian; Edd, Jon F.; Webb, Donna J.; Li, Deyu. "A microfluidic cell co-culture platform with a liquid fluorocarbon separator" BIOMEDICAL MICRODEVICES (2014)
- 129. Tegenge, Million Adane; Rajbhandari, Labchan; Shrestha, Shiva; Mithal, Aditya; Hosmane, Suneil; Venkatesan, Arun. "Curcumin protects axons from degeneration in the setting of local neuroinflammation" EXPERIMENTAL NEUROLOGY (2014)
- 130. Saito, Atsushi; Takayama, Yuzo; Moriguchi, Hiroyuki; Kotani, Kiyoshi; Jimbo, Yasuhiko. "Induced Current Pharmacological Split Stimulation System for Neuronal Networks" IEEE TRANSACTIONS ON BIOMEDICAL ENGINEERING (2014)
- 131. Tang-Schomer, Min D.; Davies, Paul; Graziano, Daniel; Thurber, Amy E.; Kaplan, David L.. "Neural circuits with long-distance axon tracts for determining functional connectivity" JOURNAL OF NEUROSCIENCE METHODS (2014)
- 132. Park, Jaewon; Kim, Sunja; Park, Su Inn; Choe, Yoonsuck; Li, Jianrong; Han, Arum. "A microchip for quantitative analysis of CNS axon growth under localized biomolecular treatments" JOURNAL OF NEUROSCIENCE METHODS (2014)
- 133. Deleglise, Berangere; Magnifico, Sebastien; Duplus, Eric; Vaur, Pauline; Soubeyre, Vanessa; Belle, Morgane; Vignes, Maeva; Viovy, Jean-Louis; Jacotot, Etienne; Peyrin, Jean-Michel; Brugg, Bernard. "beta-amyloid induces a dying-back process and remote trans-synaptic alterations in a microfluidic-based reconstructed neuronal network" ACTA NEUROPATHOLOGICA COMMUNICATIONS (2014)
- 134. Dujardin, Simon; Lecolle, Katia; Caillierez, Raphaelle; Begard, Severine; Zommer, Nadege; Lachaud, Cedrick; Carrier, Sebastien; Dufour, Noelle; Auregan, Gwennaelle; Winderickx, Joris; Hantraye, Philippe; Deglon, Nicole; Colin, Morvane; Buee, Luc. "Neuron-to-neuron wild-type Tau protein transfer through a trans-synaptic mechanism: relevance to sporadic tauopathies" ACTA NEUROPATHOLOGICA COMMUNICATIONS (2014)

- 135. Song, Ha-Lim; Shim, Sungbo; Kim, Dong-Hou; Won, Se-Hoon; Joo, Segyeong; Kim, Sudong; Jeon, Noo Li; Yoon, Seung-Yong. "beta-Amyloid Is Transmitted via Neuronal Connections along Axonal Membranes" ANNALS OF NEUROLOGY (2014)
- 136. Robertson, Graham; Bushell, Trevor J.; Zagnoni, Michele. "Chemically induced synaptic activity between mixed primary hippocampal co-cultures in a microfluidic system" INTEGRATIVE BIOLOGY (2014)
- 137. Tong, Ziqiu; Seira, Oscar; Casas, Cristina; Reginensi, Diego; Homs-Corbera, Antoni; Samitier, Josep; Antonio Del Rio, Jose. "Engineering a functional neuro-muscular junction model in a chip" RSC ADVANCES (2014)
- 138. Rage, Florence; Boulisfane, Nawal; Rihan, Khalil; Neel, Henry; Gostan, Thierry; Bertrand, Edouard; Bordonne, Remy; Soret, Johann. "Genome-wide identification of mRNAs associated with the protein SMN whose depletion decreases their axonal localization" RNA (2013)
- 139. Tsantoulas, Christoforos; Farmer, Clare; Machado, Patricia; Baba, Katsuhiro; McMahon, Stephen B.; Raouf, Ramin. "Probing Functional Properties of Nociceptive Axons Using a Microfluidic Culture System" PLOS ONE (2013)
- 140. Sauer, Brian M.; Schmalstieg, William F.; Howe, Charles L.. "Axons are injured by antigen-specific CD8(+) T cells through a MHC class I- and granzyme B-dependent mechanism" NEUROBIOLOGY OF DISEASE (2013)
- 141. Brewer, Gregory J.; Boehler, Michael D.; Leondopulos, Stathis; Pan, Liangbin; Alagapan, Sankaraleengam; DeMarse, Thomas B.; Wheeler, Bruce C.. "Toward a self-wired active reconstruction of the hippocampal trisynaptic loop: DG-CA3" FRONTIERS IN NEURAL CIRCUITS (2013)
- 142. Southam, Katherine A.; King, Anna E.; Blizzard, Catherine A.; McCormack, Graeme H.; Dickson, Tracey C.. "Microfluidic-primary culture model of the lower motor neuron-neuromuscular junction circuit" JOURNAL OF NEUROSCIENCE METHODS (2013)
- 143. Deleglise, Berangere; Lassus, Benjamin; Soubeyre, Vaneyssa; Alleaume-Butaux, Aurelie; Hjorth, Johannes J.; Vignes, Maeva; Schneider, Benoit; Brugg, Bernard; Viovy, Jean-Louis; Peyrin, Jean-Michel. "Synapto-Protective Drugs Evaluation in Reconstructed Neuronal Network" PLOS ONE (2013)
- 144. Saito, Atsushi; Saito, Aki; Moriguchi, Hiroyuki; Kotani, Kiyoshi; Jimbo, Yasuhiko. "Localized Induced Current Stimulation to Neuronal Culture Using Soft Magnetic Material" ELECTRONICS AND COMMUNICATIONS IN JAPAN (2013)
- 145. Sun, Tao; Yu, Nuo; Zhai, Lu-Kai; Li, Na; Zhang, Chao; Zhou, Liang; Huang, Zhuo; Jiang, Xing-Yu; Shen, Ying; Chen, Zhe-Yu. "c-Jun NH2-terminal Kinase (JNK)-interacting Protein-3 (JIP3) Regulates Neuronal Axon Elongation in a Kinesin- and JNK-dependent Manner" JOURNAL OF BIOLOGICAL CHEMISTRY (2013)
- 146. Ben M'Barek, Karim; Pla, Patrick; Orvoen, Sophie; Benstaali, Caroline; Godin, Juliette D.; Gardier, Alain M.; Saudou, Frederic; David, Denis J.; Humbert, Sandrine. "Huntingtin Mediates Anxiety/Depression-Related Behaviors and Hippocampal Neurogenesis" JOURNAL OF NEUROSCIENCE (2013)
- 147. Swanger, Sharon A.; He, Yuncen A.; Richter, Joel D.; Bassell, Gary J.. "Dendritic GluN2A Synthesis Mediates Activity-Induced NMDA Receptor Insertion" JOURNAL OF NEUROSCIENCE (2013)
- 148. Cusack, Corey L.; Swahari, Vijay; Henley, W. Hampton; Ramsey, J. Michael; Deshmukh, Mohanish. "Distinct pathways mediate axon degeneration during apoptosis and axon-specific pruning" NATURE COMMUNICATIONS (2013)
- 149. Zhang, Yi; Ueno, Yuji; Liu, Xian Shuang; Buller, Benjamin; Wang, Xinli; Chopp, Michael; Zhang, Zheng Gang. "The MicroRNA-17-92 Cluster Enhances Axonal Outgrowth in Embryonic Cortical Neurons" JOURNAL OF NEUROSCIENCE (2013)
- 150. Liot, Geraldine; Zala, Diana; Pla, Patrick; Mottet, Guillaume; Piel, Matthieu; Saudou, Frederic. "Mutant Huntingtin Alters Retrograde Transport of TrkB Receptors in Striatal Dendrites" JOURNAL OF NEUROSCIENCE (2013)
- 151. Zala, Diana; Hinckelmann, Maria-Victoria; Saudou, Frederic. "Huntingtin's Function in Axonal Transport Is Conserved in Drosophila melanogaster" PLOS ONE (2013)
- 152. Taylor, Anne Marion; Wu, Jason; Tai, Hwan-Ching; Schuman, Erin M.. "Axonal Translation of beta-Catenin Regulates Synaptic Vesicle Dynamics" JOURNAL OF NEUROSCIENCE (2013)
- 153. Sgro, Allyson E.; Bajjalieh, Sandra M.; Chiu, Daniel T.. "Single-Axonal Organelle Analysis Method Reveals New Protein-Motor Associations" ACS CHEMICAL NEUROSCIENCE (2013)
- 154. Barbati, Alexander C.; Fang, Cheng; Banker, Gary A.; Kirby, Brian J.. "Culture of primary rat hippocampal neurons: design, analysis, and optimization of a microfluidic device for cell seeding, coherent growth, and solute delivery" BIOMEDICAL MICRODEVICES (2013)
- 155. Wu, Jessica W.; Herman, Mathieu; Liu, Li; Simoes, Sabrina; Acker, Christopher M.; Figueroa, Helen; Steinberg, Joshua I.; Margittai, Martin; Kayed, Rakez; Zurzolo, Chiara; Di Paolo, Gilbert; Duff, Karen E.. "Small Misfolded Tau Species Are Internalized via Bulk Endocytosis and Anterogradely and Retrogradely Transported in Neurons" JOURNAL OF BIOLOGICAL CHEMISTRY (2013)
- 156. Shimba, Kenta; Sakai, Koji; Arimatsu, Kazuyuki; Kotani, Kiyoshi; Jimbo, Yasuhiko. "Long Term Observation of Propagating Action Potentials along the Axon in a Microtunnel Device" 2013 6TH INTERNATIONAL IEEE/EMBS CONFERENCE ON NEURAL ENGINEERING (NER) (2013)

- 157. Nguyen, Thanh D.; Hogue, Ian B.; Cung, Kellye; Purohit, Prashant K.; McAlpine, Michael C.. "Tension-induced neurite growth in microfluidic channels" LAB ON A CHIP (2013)
- 158. Honegger, Thibault; Scott, Mark A.; Yanik, Mehmet F.; Voldman, Joel. "Electrokinetic confinement of axonal growth for dynamically configurable neural networks" LAB ON A CHIP (2013)
- 159. Hallfors, Nicholas; Khan, Asif; Dickey, Michael D.; Taylor, Anne Marion. "Integration of pre-aligned liquid metal electrodes for neural stimulation within a user-friendly microfluidic platform" LAB ON A CHIP (2013)
- 160. Ngoc-Duy Dinh; Chiang, Ya-Yu; Hardelauf, Heike; Baumann, Jenny; Jackson, Emily; Waide, Sarah; Sisnaiske, Julia; Frimat, Jean-Philippe; van Thriel, Christoph; Janasek, Dirk; Peyrin, Jean-Michel; West, Jonathan. "Microfluidic construction of minimalistic neuronal co-cultures" LAB ON A CHIP (2013)
- 161. Grigoryan, Sergei; Kinchington, Paul R.; Yang, In Hong; Selariu, Anca; Zhu, Hua; Yee, Michael; Goldstein, Ronald S.. "Retrograde axonal transport of VZV: kinetic studies in hESC-derived neurons" JOURNAL OF NEUROVIROLOGY (2012)
- 162. Butko, Margaret T.; Yang, Jin; Geng, Yang; Kim, Hyung Joon; Jeon, Noo Li; Shu, Xiaokun; Mackey, Mason R.; Ellisman, Mark H.; Tsien, Roger Y.; Lin, Michael Z.. "Fluorescent and photo-oxidizing TimeSTAMP tags track protein fates in light and electron microscopy" NATURE NEUROSCIENCE (2012)
- 163. Walker, Breset A.; Ji, Sheng-Jian; Jaffrey, Samie R.. "Intra-Axonal Translation of RhoA Promotes Axon Growth Inhibition by CSPG" JOURNAL OF NEUROSCIENCE (2012)
- 164. Freundt, Eric C.; Maynard, Nate; Clancy, Eileen K.; Roy, Shyamali; Bousset, Luc; Sourigues, Yannick; Covert, Markus; Melki, Ronald; Kirkegaard, Karla; Brahic, Michel. "Neuron-to-neuron transmission of alpha-synuclein fibrils through axonal transport" ANNALS OF NEUROLOGY (2012)
- 165. Li, Li; Ren, Li; Liu, Wenming; Wang, Jian-Chun; Wang, Yaolei; Tu, Qin; Xu, Juan; Liu, Rui; Zhang, Yanrong; Yuan, Mao-Sen; Li, Tianbao; Wang, Jinyi. "Spatiotemporally Controlled and Multifactor Involved Assay of Neuronal Compartment Regeneration after Chemical Injury in an Integrated Microfluidics" ANALYTICAL CHEMISTRY (2012)
- 166. Lu, Xi; Kim-Han, Jeong S.; O'Malley, Karen L.; Sakiyama-Elbert, Shelly E.. "A microdevice platform for visualizing mitochondrial transport in aligned dopaminergic axons" JOURNAL OF NEUROSCIENCE METHODS (2012)
- 167. Fujiwara, Takeshi; Morimoto, Koji. "Cooperative effect of p150Glued and microtubule stabilization to suppress excitotoxicity-induced axon degeneration" BIOCHEMICAL AND BIOPHYSICAL RESEARCH COMMUNICATIONS (2012)
- 168. Kobayashi, Mariko; Wilson, Angus C.; Chao, Moses V.; Mohr, Ian. "Control of viral latency in neurons by axonal mTOR signaling and the 4E-BP translation repressor" GENES & DEVELOPMENT (2012)
- 169. Kim, Hyung Joon; Park, Jeong Won; Byun, Jae Hwan; Poon, Wayne W.; Cotman, Carl W.; Fowlkes, Charless C.; Jeon, Noo Li. "Quantitative Analysis of Axonal Transport by Using Compartmentalized and Surface Micropatterned Culture of Neurons" ACS CHEMICAL NEUROSCIENCE (2012)
- 170. Yang, In Hong; Gary, Devin; Malone, Misti; Dria, Stephen; Houdayer, Thierry; Belegu, Visar; Mcdonald, John W.; Thakor, Nitish. "Axon Myelination and Electrical Stimulation in a Microfluidic, Compartmentalized Cell Culture Platform" NEUROMOLECULAR MEDICINE (2012)
- 171. Hosmane, Suneil; Tegenge, Million Adane; Rajbhandari, Labchan; Uapinyoying, Prech; Kumar, Nishant Ganesh; Thakor, Nitish; Venkatesan, Arun. "Toll/Interleukin-1 Receptor Domain-Containing Adapter Inducing Interferon-beta Mediates Microglial Phagocytosis of Degenerating Axons" JOURNAL OF NEUROSCIENCE (2012)
- 172. Ueno, Masaki; Hayano, Yasufumi; Nakagawa, Hiroshi; Yamashita, Toshihide. "Intraspinal rewiring of the corticospinal tract requires target-derived brain-derived neurotrophic factor and compensates lost function after brain injury" BRAIN (2012)
- 173. Wang, Ling; Riss, Michael; Buitrago, Jennifer Olmos; Claverol-Tinture, Enric. "Biophysics of microchannel-enabled neuron-electrode interfaces" JOURNAL OF NEURAL ENGINEERING (2012)
- 174. Zhang, Yanqing; Bekku, Yoko; Dzhashiashvili, Yulia; Armenti, Stephen; Meng, Xiaosong; Sasaki, Yo; Milbrandt, Jeffrey; Salzer, James L.. "Assembly and Maintenance of Nodes of Ranvier Rely on Distinct Sources of Proteins and Targeting Mechanisms" NEURON (2012)
- 175. Park, Jaewon; Koito, Hisami; Li, Jianrong; Han, Arum. "Multi-compartment neuron-glia co-culture platform for localized CNS axon-glia interaction study" LAB ON A CHIP (2012)
- 176. Takayama, Yuzo; Moriguchi, Hiroyuki; Kotani, Kiyoshi; Suzuki, Takafumi; Mabuchi, Kunihiko; Jimbo, Yasuhiko.
 "Network-wide integration of stem cell-derived neurons and mouse cortical neurons using microfabricated co-culture devices" BIOSYSTEMS (2012)
- 177. Hosie, Katherine A.; King, Anna E.; Blizzard, Catherine A.; Vickers, James C.; Dickson, Tracey C.. "Chronic excitotoxin-induced axon degeneration in a compartmented neuronal culture model" ASN NEURO (2012)
- 178. Volpicelli-Daley, Laura A.; Luk, Kelvin C.; Patel, Tapan P.; Tanik, Selcuk A.; Riddle, Dawn M.; Stieber, Anna; Meaney, David F.; Trojanowski, John Q.; Lee, Virginia M. -Y.. "Exogenous alpha-Synuclein Fibrils Induce Lewy Body Pathology Leading to Synaptic Dysfunction and Neuron Death" NEURON (2011)

- 179. Shi, Peng; Scott, Mark A.; Ghosh, Balaram; Wan, Dongpeng; Wissner-Gross, Zachary; Mazitschek, Ralph; Haggarty, Stephen J.; Yanik, Mehmet Fatih. "Synapse microarray identification of small molecules that enhance synaptogenesis" NATURE COMMUNICATIONS (2011)
- 180. Pan, Liangbin; Alagapan, Sankaraleengam; Franca, Eric; Brewer, Gregory J.; Wheeler, Bruce C.. "Propagation of action potential activity in a predefined microtunnel neural network" JOURNAL OF NEURAL ENGINEERING (2011)
- 181. Cohen, Michael S.; Orth, Carlos Bas; Kim, Hyung Joon; Jeon, Noo Li; Jaffrey, Samie R.. "Neurotrophin-mediated dendrite-to-nucleus signaling revealed by microfluidic compartmentalization of dendrites" PROCEEDINGS OF THE NATIONAL ACADEMY OF SCIENCES OF THE UNITED STATES OF AMERICA (2011)
- 182. Andres, Robert H.; Horie, Nobutaka; Slikker, William; Keren-Gill, Hadar; Zhan, Ke; Sun, Guohua; Manley, Nathan C.; Pereira, Marta P.; Sheikh, Lamiya A.; McMillan, Erin L.; Schaar, Bruce T.; Svendsen, Clive N.; Bliss, Tonya M.; Steinberg, Gary K.. "Human neural stem cells enhance structural plasticity and axonal transport in the ischaemic brain" BRAIN (2011)
- 183. Hur, Eun-Mi; Yang, In Hong; Kim, Deok-Ho; Byun, Justin; Saijilafu; Xu, Wen-Lin; Nicovich, Philip R.; Cheong, Raymond; Levchenko, Andre; Thakor, Nitish; Zhou, Feng-Quan. "Engineering neuronal growth cones to promote axon regeneration over inhibitory molecules" PROCEEDINGS OF THE NATIONAL ACADEMY OF SCIENCES OF THE UNITED STATES OF AMERICA (2011)
- 184. Pirlo, R. K.; Sweeney, A. J.; Ringeisen, B. R.; Kindy, M.; Gao, B. Z.. "Biochip/laser cell deposition system to assess polarized axonal growth from single neurons and neuron/glia pairs in microchannels with novel asymmetrical geometries" BIOMICROFLUIDICS (2011)
- 185. Danzer, Karin M.; Ruf, Wolfgang P.; Putcha, Preeti; Joyner, Daniel; Hashimoto, Tadafumi; Glabe, Charles; Hyman, Bradley T.; McLean, Pamela J.. "Heat-shock protein 70 modulates toxic extracellular alpha-synuclein oligomers and rescues trans-synaptic toxicity" FASEB JOURNAL (2011)
- 186. Arundell, Martin; Perry, V. Hugh; Newman, Tracey. A.. "Integration of a macro/micro architectured compartmentalised neuronal culture device using a rapid prototyping moulding process" LAB ON A CHIP (2011)
- 187. Peyrin, Jean-Michel; Deleglise, Berangere; Saias, Laure; Vignes, Maeva; Gougis, Paul; Magnifico, Sebastien; Betuing, Sandrine; Pietri, Mathea; Caboche, Jocelyne; Vanhoutte, Peter; Viovy, Jean-Louis; Brugg, Bernard. "Axon diodes for the reconstruction of oriented neuronal networks in microfluidic chambers" LAB ON A CHIP (2011)
- 188. Hosmane, Suneil; Fournier, Adam; Wright, Rika; Rajbhandari, Labchan; Siddique, Rezina; Yang, In Hong; Ramesh, K. T.; Venkatesan, Arun; Thakor, Nitish. "Valve-based microfluidic compression platform: single axon injury and regrowth" LAB ON A CHIP (2011)
- 189. Kilinc, Devrim; Peyrin, Jean-Michel; Soubeyre, Vanessa; Magnifico, Sebastien; Saias, Laure; Viovy, Jean-Louis; Brugg, Bernard. "Wallerian-Like Degeneration of Central Neurons After Synchronized and Geometrically Registered Mass Axotomy in a Three-Compartmental Microfluidic Chip" NEUROTOXICITY RESEARCH (2011)
- 190. Taylor, Anne M.; Dieterich, Daniela C.; Ito, Hiroshi T.; Kim, Sally A.; Schuman, Erin M.. "Microfluidic Local Perfusion Chambers for the Visualization and Manipulation of Synapses" NEURON (2010)
- 191. Vitzthum, Lucas; Chen, Xinzhi; Kintner, Douglas B.; Huang, Yu; Chiu, Shing-Yan; Williams, Justin; Sun, Dandan. "Study of Na+/H+ exchange-mediated pH(i) regulations in neuronal soma and neurites in compartmentalized microfluidic devices" INTEGRATIVE BIOLOGY (2010)
- 192. Hosmane, Suneil; Yang, In Hong; Ruffin, April; Thakor, Nitish; Venkatesan, Arun. "Circular compartmentalized microfluidic platform: Study of axon-glia interactions" LAB ON A CHIP (2010)
- Berdichevsky, Yevgeny; Staley, Kevin J.; Yarmush, Martin L.. "Building and manipulating neural pathways with microfluidics" LAB ON A CHIP (2010)
- 194. Shi, Peng; Nedelec, Stephane; Wichterle, Hynek; Kam, Lance C.. "Combined microfluidics/protein patterning platform for pharmacological interrogation of axon pathfinding" LAB ON A CHIP (2010)
- 195. Zhang, Kai; Osakada, Yasuko; Vrljic, Marija; Chen, Liang; Mudrakola, Harsha V.; Cui, Bianxiao. "Single-molecule imaging of NGF axonal transport in microfluidic devices" LAB ON A CHIP (2010)
- 196. Park, Jaewon; Koito, Hisami; Li, Jianrong; Han, Arum. "Microfluidic compartmentalized co-culture platform for CNS axon myelination research" BIOMEDICAL MICRODEVICES (2009)
- 197. Shulga, Anastasia; Blaesse, Anne; Kysenius, Kai; Huttunen, Henri J.; Tanhuanpaa, Kimmo; Saarma, Mart; Rivera, Claudio. "Thyroxin regulates BDNF expression to promote survival of injured neurons" MOLECULAR AND CELLULAR NEUROSCIENCE (2009)
- 198. Stoothoff, Will; Jones, Phillip B.; Spires-Jones, Tara L.; Joyner, Daniel; Chhabra, Ekta; Bercury, Kathryn; Fan, Zhanyun; Xie, Hong; Bacskai, Brian; Edd, Jon; Irimia, Daniel; Hyman, Bradley T.. "Differential effect of three-repeat and four-repeat tau on mitochondrial axonal transport" JOURNAL OF NEUROCHEMISTRY (2009)
- 199. Blurton-Jones, Mathew; Kitazawa, Masashi; Martinez-Coria, Hilda; Castello, Nicholas A.; Mueller, Franz-Josef; Loring, Jeanne F.; Yamasaki, Tritia R.; Poon, Wayne W.; Green, Kim N.; LaFerla, Frank M.. "Neural stem cells improve cognition via BDNF in a transgenic model of Alzheimer disease" PROCEEDINGS OF THE NATIONAL ACADEMY OF SCIENCES OF THE UNITED STATES OF AMERICA (2009)

- 200. Hengst, Ulrich; Deglincerti, Alessia; Kim, Hyung Joon; Jeon, Noo Li; Jaffrey, Samie R.. "Axonal elongation triggered by stimulus-induced local translation of a polarity complex protein" NATURE CELL BIOLOGY (2009)
- 201. Yang, In Hong; Siddique, Rezina; Hosmane, Suneil; Thakor, Nitish; Hoeke, Ahmet. "Compartmentalized microfluidic culture platform to study mechanism of paclitaxel-induced axonal degeneration" EXPERIMENTAL NEUROLOGY (2009)
- 202. Taylor, Anne M.; Berchtold, Nicole C.; Perreau, Victoria M.; Tu, Christina H.; Jeon, Noo Li; Cotman, Carl W.. "Axonal mRNA in Uninjured and Regenerating Cortical Mammalian Axons" JOURNAL OF NEUROSCIENCE (2009)
- 203. Berdichevsky, Yevgeny; Sabolek, Helen; Levine, John B.; Staley, Kevin J.; Yarmush, Martin L.. "Microfluidics and multielectrode array-compatible organotypic slice culture method" JOURNAL OF NEUROSCIENCE METHODS (2009)
- 204. Kim, Young-tae; Karthikeyan, Kailash; Chirvi, Sajal; Dave, Digant P.. "Neuro-optical microfluidic platform to study injury and regeneration of single axons" LAB ON A CHIP (2009)
- 205. Liu, Wendy W.; Goodhouse, Joseph; Jeon, Noo Li; Enquist, L. W.. "A Microfluidic Chamber for Analysis of Neuron-to-Cell Spread and Axonal Transport of an Alpha-Herpesvirus" PLOS ONE (2008)
- 206. Bergen, Jamie M.; Pun, Suzie H.. "Analysis of the intraceltular barriers encountered by nonviral gene carriers in a model of spatially controlled delivery to neurons" JOURNAL OF GENE MEDICINE (2008)
- 207. Cui, Bianxiao; Wu, Chengbiao; Chen, Liang; Ramirez, Alfredo; Bearer, Elaine L.; Li, Wei-Ping; Mobley, William C.; Chu, Steven. "One at a time, live tracking of NGF axonal transport using quantum dots" PROCEEDINGS OF THE NATIONAL ACADEMY OF SCIENCES OF THE UNITED STATES OF AMERICA (2007)
- 208. Sutton, Michael A.; Taylor, Anne M.; Ito, Hiroshi T.; Pham, Anh; Schuman, Erin M.. "Postsynaptic decoding of neural activity: eEF2 as a biochemical sensor coupling miniature synaptic transmission to local protein synthesis" NEURON (2007)
- 209. Millet, Larry J.; Stewart, Matthew E.; Sweedler, Jonathan V.; Nuzzo, Ralph G.; Gillette, Martha U.. "Microfluidic devices for culturing primary mammalian neurons at low densities" LAB ON A CHIP (2007)
- 210. Ding, JQ; Allen, E; Wang, W; Valle, A; Wu, CB; Nardine, T; Cui, BX; Yi, J; Taylor, A; Jeon, NL; Chu, S; So, Y; Vogel, H; Tolwani, R; Mobley, W; Yang, YM. "Gene targeting of GAN in mouse causes a toxic accumulation of microtubule-associated protein 8 and impaired retrograde axonal transport" HUMAN MOLECULAR GENETICS (2006)
- 211. Park, Jeong Won; Vahidi, Behrad; Taylor, Anne M.; Rhee, Seog Woo; Jeon, Noo Li. "Microfluidic culture platform for neuroscience research" NATURE PROTOCOLS (2006)